https://doi.org/10.5194/egusphere-2026-4883
Preprint. Discussion started: 14 August 2026

Tropospheric Oxidation Chemistry and Methane Growth: A Process-Based Attribution of OH Variability (2003–2022)

Benjamin Gaubert[1,*], Mohammad Amin Mirrezaei[2,*], Rafael P. Fernandez[3,4], Ivan Ortega[1], Louisa Emmons[1], John Orlando[1], Youmi Oh[5,6], Lori Bruhwiler[5], Shuo Chen[7], Gabrielle Pétron[5], Xin Lan[5,6], Claire Granier[6,8,9], Nicolas Zilbermann[10], Idir Bouarar[11], Guy P. Brasseur[1,11], Chuan Feng[12], Yangyang Xu[12], Alfonso Saiz-Lopez[13], Carlos A. Cuevas[13], and Avelino F. Arellano Jr.[2]

[1]Atmospheric Chemistry Observations & Modeling Laboratory (ACOM), NSF National Center for Atmospheric Research (NSF NCAR), Boulder, CO, USA
[2]Department of Hydrology and Atmospheric Sciences, University of Arizona, AZ, USA
[3]School of Natural Sciences, National University of Cuyo (FCEN-UNCuyo), Mendoza, Argentina
[4]Institute for Interdisciplinary Science, National Research Council (ICB-CONICET), Mendoza, Argentina
[5]NOAA Global Monitoring Laboratory, Boulder, CO, USA
[6]Cooperative Institute for Research in Environmental Sciences, University of Colorado Boulder, Boulder, CO, USA
[7]Department of Earth, Atmospheric, and Planetary Sciences, Purdue University, West Lafayette, IN, USA
[8]NOAA Chemical Sciences Laboratory, Boulder, CO
[9]Laboratoire d'Aérologie, CNRS, Université de Toulouse, Toulouse, France
[10]Observatoire Midi-Pyrénées, Toulouse, France
[11]Max-Planck Institute for Meteorology, Hamburg, Germany
[12]Department of Atmospheric Sciences, Texas A&M University, College Station, Texas, USA
[13]Department of Atmospheric Chemistry and Climate, Institute of Physical Chemistry Blas Cabrera, CSIC, Madrid, Spain
[*]These authors contributed equally to this work.

Correspondence: Benjamin Gaubert (gaubert@ucar.edu) and Mohammad Amin Mirrezaei (amirrezaei@arizona.edu)

Abstract. Earth system models that include interactive chemistry provide a mechanistic understanding of the hydroxyl radical (OH) sources and sinks. However, their use is often limited in the estimation of the global methane (CH_4) budget. We conduct 20-year emission-driven methane simulations (2003-2022) with the Community Earth System Model Version 2.2 (CESM2.2) nudged to different meteorological datasets and input various chemical emissions, including the Seventh Coupled Model Intercomparison Project (CMIP7). Our evaluation includes in-situ observations from the NOAA Marine Boundary Layer Reference and airborne field studies, as well as ground-based and satellite remote sensing observations of carbon monoxide (CO) and CH_4. We find that the model configurations with a lower OH bias have improved skill in reproducing both CO and CH_4 spatial and temporal variations, including the CH_4 annual growth rate. We quantify the OH impacts on the CH_4 growth rate and derive a comprehensive attribution of OH changes to Earth System chemical processes. Despite an interannual variability lower than 4 %, changes in OH explains around 30 % of the interannual variability of the CH_4 growth throughout the 2003-2022 period. The OH changes arise from both internal variability —via biogenic and lightning emission responses— and prescribed surface emissions, with remaining uncertainties. We find that OH is well buffered against chemistry perturbations, as increased chemical complexity raises the OH recycling probability. Consequently, studies relying on simplified and prescribed OH repre-

https://doi.org/10.5194/egusphere-2026-4883
Preprint. Discussion started: 14 August 2026

sentations may neglect these complex chemical feedbacks and overestimate the role of OH changes in driving the CH_4 growth rate.

1 Introduction

Changes in atmospheric methane (CH_4) abundance depend on the balance between surface emissions and loss through microbial uptake in soils and atmospheric oxidation. Direct emissions from human activities such as fossil fuel production, agriculture activities such as livestock production and rice cultivation, and waste disposal, account for around 65 % of the total emissions (Saunois et al., 2025). The remaining sources are natural and are dominated by tropical and high latitude wetlands (e.g., Xiao et al., 2024), with minor contributions from fires, terrestrial permafrost, wild animals, termites, geological sources, as well as anthropogenic sources considered indirect, resulting from CH_4 emissions from water stagnating in dams and reservoirs. Given the large uncertainties and diversity of sources, the spatial and temporal variation of emissions are often estimated using Bayesian inverse models that combined prior flux estimates with CH_4 observations (e.g., Worden et al., 2023). Observational constraints on global methane budget include in-situ CH_4 mixing ratios and its isotopic ratio (^{13}C:^{12}C), denoted as δ^{13}C-CH_4 (Lan et al., 2021a), its deuterium to hydrogen isotopic ratio (^{2}H:^{1}H), denoted as δD-CH_4 (Riddell-Young et al., 2025), as well as satellite retrievals of atmospheric column concentrations (Jacob et al., 2022) such as the Greenhouse Gases Observing Satellite (GOSAT) launched in 2009 and the TROpospheric Monitoring Instrument (TROPOMI) since 2018.

Since 2000, changes in the atmospheric CH_4 growth rate have been characterized by a 'pause' (1999 to 2006) of near-constant CH_4 atmospheric abundance, followed by 'renewed growth' starting in 2007, with periods of 'acceleration' when the global and annual CH_4 growth rate was higher than 10 ppb yr^{-1} (Rigby et al., 2008; Dlugokencky et al., 2009; Nisbet et al., 2019, 2023; Nisbet and Manning, 2026). The inclusion of δ^{13}C-CH_4 and δD-CH_4 measurements in flux inversions implies that the increase in microbial emissions explains most of the 2006-2022 increase in atmospheric CH_4 growth rate (Thompson et al., 2018; Basu et al., 2022; Michel et al., 2024; Riddell-Young et al., 2025; Oh et al., 2026; Yu et al., 2026). This is hypothesized to be driven by larger emissions from wetter and warmer tropical wetlands driven by precipitation and temperature increases during negative phases of the El Niño–Southern Oscillation (ENSO), i.e., La Niña years (Hodson et al., 2011; Zhu et al., 2017; Dean et al., 2018; Zhang et al., 2023). This is further corroborated by improved wetland carbon isotopic signature maps (Oh et al., 2022) and satellite-based inversions (Yin et al., 2021; Qu et al., 2024). Increases in farmed animals, waste management, and coal mining in China may have further contributed to the CH_4 rise since 2006 (Chandra et al., 2024). Recent studies indicate that an increases in CH_4 emissions during the 2019–2024 period are attributed to livestock, waste, and wetlands, dominated by sources in South America and Africa (He et al., 2026; Balasus et al., 2026). Yu et al. (2026) assimilated TROPOMI and CH_4 isotopologues observations and found larger fossil fuel increase in China and a relative decrease of wetland CH_4 emissions from the Amazon Basin.

The hydroxyl radical OH· (hereafter denoted as OH for brevity) is the most important oxidant of the troposphere and thus controls the chemical loss of many species including carbon monoxide (CO) and CH_4 (Levy, 1971). The primary source of OH is the reaction of water vapor (H_2O) with the excited oxygen atom $O(^1D)$, produced by ozone (O_3) photolysis for wavelengths

https://doi.org/10.5194/egusphere-2026-4883
Preprint. Discussion started: 14 August 2026

smaller than 330 nm:

$$O_3 + h\nu(\lambda < 330nm) \rightarrow O(^1D) + O_2 \quad \text{(R1)}$$

$$O(^1D) + H_2O \rightarrow OH + OH \quad \text{(R2)}$$

As this reaction alone constitutes 50 to 60 % of the OH sources, temperature, water vapor (expressed as specific humidity), and shortwave radiation reaching the troposphere (dependent on overhead O_3 in the stratosphere, driving $O(^1D)$ production) are all important direct drivers of OH (e.g., Holmes et al., 2013). The main OH losses are through its reaction with CO, CH_4 and isoprene in the lower troposphere across the tropics (Fiore et al., 2006; Lelieveld et al., 2016; Yoon et al., 2025). Early modeling studies suggested that large increases in CH_4 and, to a lesser extent, carbon monoxide (CO) during the second half of the 20^{th} century could diminish the Earth's oxidation efficiency, defined as the globally averaged OH abundance (Crutzen and Zimmermann, 1991), if insufficient O_3 is produced during their oxidation (e.g., Logan et al., 1981). Thompson (1992) identified an increasing trend in tropospheric O_3 due to increases in precursor emissions, e.g., CH_4, CO, and non-methane hydrocarbons (NMHC). However, they could not easily identify OH trends due to the difficulty of balancing the concomitant increases in OH sources (O_3) and sinks (CO, CH_4).

The latest chemistry–climate model assessments, including AeroChemMIP as part of the Phase 6 of the Coupled Model Intercomparison Project (CMIP6), indicate that the rise in tropospheric O_3 since pre-industrial times is driven by increased anthropogenic sources rather than climate variability (Turnock et al., 2020; Griffiths et al., 2021; Fiore et al., 2022). Driven by economic activities, the increase in precursor emissions at lower latitudes of the Northern Hemisphere (NH), ongoing since the 1980s, has led to positive O_3 trends across the tropics, including the upper troposphere (Zhang et al., 2016; Yu et al., 2024; Froidevaux et al., 2025). As a result, chemistry–climate models tend to produce a net positive trend in OH since 1980 (Naik et al., 2013; Stevenson et al., 2020), driven by increasing O_3, nitrogen oxides (NO_x) and water vapor (Nicely et al., 2018; Chua et al., 2023), and decreasing anthropogenic CO emissions and abundance (Gaubert et al., 2017). Larger source of CH_4 contributes to the tropospheric O_3 growth and acts as a net sink for OH (Lelieveld et al., 1998; Shindell et al., 2005). Future OH abundance depends on which Shared Socioeconomic Pathway (SSP) emission scenarios is used, where decreases in CO and CH_4 in the strong climate mitigation scenario (SSP1-2.6) are projected to reduce OH losses, increase OH, and thus further reduce the CH_4 lifetime. Staniaszek et al. (2022) performed simulations with a CH_4 emissions-driven version (Folberth et al., 2022) of the UK Earth System Model (UKESM1) and found that a hypothetical abatement of all CH_4 anthropogenic emissions caused a reduction in CO and hydroperoxyl radical (HO_2), slowing O_3 production and its role as OH source, yet still with increases in OH larger than 30 % due to the reduction of both CH_4 and CO. Aerosols, short-lived gases, and CH_4 act together to shape near-term climate and air quality. Allen et al. (2021) estimated that CH_4 mitigation could offset the warming induced by aerosol reductions while improving air quality.

While chemistry climate models simulate lower OH interannual variability (0.9 % to 1.8 % over 2000–2010, Saunois et al., 2025), observationally derived estimates suggest an interannual variability around 2 to 3 % (e.g., Montzka et al., 2011; Patra et al., 2021; Yin et al., 2021). This contradiction has led to some skepticism about the use of global chemistry models to

https://doi.org/10.5194/egusphere-2026-4883
Preprint. Discussion started: 14 August 2026

assess the role of OH in the CH_4 budget (Turner et al., 2019). However, methyl chloroform-based estimates are also subject to errors, in particular in two-box model inversions, allowing for both positive and negative OH trends within the uncertainty range (Rigby et al., 2017; Turner et al., 2017; Naus et al., 2019). As the declining atmospheric abundance of methyl chloroform reduces its ability to constrain OH for more recent periods, Thompson et al. (2024) used five hydrofluorocarbons as alternatives and found no significant OH trends, with a small interannual variability of less than 2 %. Using Southern Hemisphere measurements of radiocarbon monoxide (^{14}CO), a tracer produced by cosmic rays, (Morgenstern et al., 2025) found a declining ^{14}CO since 1997 at two remote location, one in New Zealand and one in Antarctica. It implies that OH has been increasing in the southern hemisphere in recent decades. In this context, recent work has incorporated interannually varying OH fields, rather than climatological means (Patra et al., 2011), in light of the record-high CH_4 growth rate during the early 2020s (e.g., Chen et al., 2025; Zhao et al., 2025b; Ciais et al., 2026). The inclusion of OH interannual variability and trends for other periods is acknowledged to have a significant impact on inverted emissions (e.g., Zhao et al., 2020; Belikov et al., 2026; Feng et al., 2026).

A more complete treatment of atmospheric chemistry is central to this effort. Improving this representation is key to CH_4 predictability within Earth system modelling frameworks (e.g., Folberth et al., 2025), and ultimately to Earth system predictability through a more complete understanding of the role of multi-scale chemistry processes as well as Earth system component interactions and feedbacks (Richter et al., 2026). Resolving the interaction across scales relevant for air quality and global trends would further support more accurate and efficient mitigation policy (Akimoto and Tanimoto, 2022). The inclusion of short-lived halogen (SLH) chemistry (e.g., Fernandez et al., 2025; Saiz-Lopez et al., 2025) has recently led to an important reduction in OH biases in the Community Earth System Model version 2.2 (CESM2.2), improving CH_4 prediction as well as CO in the NH during winter and spring (Mirrezaei et al., 2025). The non-linear response of the CH_4-CO-OH chemical coupling alters how the CH_4 lifetime responds to an emission perturbation, which must be accurately represented to better quantify changes in CH_4 abundance. Notably, this inclusion of SLH chemistry reduced the global annual mean feedback factor (how much CH_4 lengthens its own atmospheric lifetime through its effect on OH) from 1.29 to 1.18, at the lower end of literature estimates (Szopa et al., 2021). However, it also highlights a positive feedback through the Cl-driven oxidation pathways now quantified in SLH simulations and the total feedback factor including both Cl and OH is 1.34. More broadly, there is an urgent need to understand the interactions across spatial and temporal scales of the chemical fluxes involved in the sources and sinks of atmospheric oxidants, to reconcile modelled and observationally constrained estimates and to ultimately reduce uncertainties in OH across timescales (Szopa et al., 2021; Tan et al., 2026). Here, using a model with interactive chemistry, we identify and quantify the dynamical and chemical processes driving OH interannual variability and their impact on CH_4 growth rate, including previously overlooked anomalies. This allows us to assess the role of chemistry and CH_4 emissions in determining the atmospheric growth of CH_4, and to evaluate whether simplified OH representations adequately capture these processes.

Building on these recent model developments, we assess the role of meteorology and emissions in OH and CH_4 variability and trends using a set of emission-driven CH_4 simulations with CESM2.2. Specifically, we employ different sets of emissions of chemical species, including the newly released CMIP7 inventory, allowing us to contrast the role of anthropogenic and fire sources on the simulated tropospheric chemistry system. To evaluate the role of prescribed meteorological conditions, we also

https://doi.org/10.5194/egusphere-2026-4883
Preprint. Discussion started: 14 August 2026

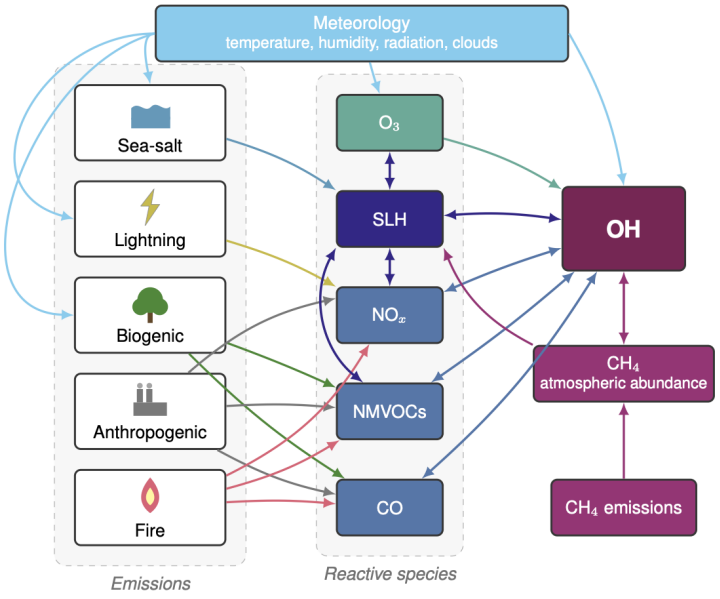

Figure 1. Schematic of the principal emission and chemical controls on tropospheric OH and their coupling to the methane budget. The chemical emission source categories (sea-salt aerosols, lightning, biogenic, anthropogenic, and fire) are displayed on the left and the main reactive species interacting with OH are in the middle row. Note that the model will include many interactions within the reactive species and OH and other species not shown here. Here we illustrates how central the short-lived halogens (SLH) are tightly coupled with the various catalytic cycles. Meteorology (temperature, humidity, radiation, clouds) regulates photolysis rates, water vapor, and reaction kinetics, and additionally drives the biogenic, lightning sources and sea-salt sources interactively . At the bottom right, the balance between methane emissions, OH and Cl losses sets the atmospheric CH_4 burden.

perform simulations with two different reanalysis datasets, the MERRA-2 (Modern-Era Retrospective analysis for Research and Applications, Version 2, Gelaro et al., 2017) and the fifth-generation ECMWF atmospheric reanalysis (ERA5, Hersbach et al., 2020). Figure 1 displays a simplified representation of the possible interaction and pathways impacting OH in our various simulations. The different meteorological forcings will impact directly the chemical species, or indirectly thought changes in
120 weather-driven emissions processes driving sea-salt, lightning and vegetation sources. Anthropogenic and fire emissions will impact non methane volatile organic compounds (NMVOCs), nitrogen oxides (NO and NO_2, NO_x), and CO. We present a thorough evaluation of the simulated CO and CH_4, as well as a detailed investigation of the chemical fluxes across these model configurations.

https://doi.org/10.5194/egusphere-2026-4883
Preprint. Discussion started: 14 August 2026

Table 1. Description of simulation experiments and input forcings. Presc. stands for CMIP6 prescribed CH_4 experiment, with SSP scenarios after 2015. CT-CH4-2025 means (NOAA CarbonTracker-CH4 2025, Oh et al., 2025). The MOPITT inversions are the results from Gaubert et al. (2024). CEDS-CMIP refers to CEDS-CMIP-2025-04-18 and CAMS-MOSAIC refers to CAMS-GLOB-ANT_m1.1. FINN2.5 refers to the Fire INventory from NCAR version 2.5 (Wiedinmyer et al., 2023), and BB4CMIP7-2-1 refers to the biomass-burning emissions dataset prepared for CMIP7 (BB4CMIP7, version 2-1). CEDS-CMIPx1.3 denotes the CEDS-CMIP anthropogenic CO emissions scaled by a factor of 1.3 (a 30% increase).

Simulation name	Meteorology	CH_4 treatment	Anthro Emiss.	Fire Emiss.	Anthro CO emiss.
CESM	MERRA-2	presc. (SSP-434)	CAMS-MOSAIC	FINN2.5	MOPITT inv.
CESM-245	MERRA-2	presc. (SSP-245)	CAMS-MOSAIC	FINN2.5	MOPITT inv.
CESM-CH4	MERRA-2	CT-CH4-2025	CAMS-MOSAIC	FINN2.5	MOPITT inv.
CESM-CH4-CMIP7	MERRA-2	CT-CH4-2025	CEDS-CMIP	BB4CMIP7-2-1	CEDS-CMIP
CESM-CH4-CMIP7-CO	MERRA-2	CT-CH4-2025	CEDS-CMIP	BB4CMIP7-2-1	CEDS-CMIPx1.3
CESM-CH4-CMIP7-ERA5	ERA5	CT-CH4-2025	CEDS-CMIP	BB4CMIP7-2-1	CEDS-CMIP
CESM-CH4-CMIP7-CO-ERA5	ERA5	CT-CH4-2025	CEDS-CMIP	BB4CMIP7-2-1	CEDS-CMIPx1.3
CESM-CH4-2003	MERRA-2	CT-CH4-2025 (2003)	CAMS-MOSAIC	FINN2.5	MOPITT inv.

2 Methods

2.1 Community Atmosphere Model with chemistry (CAM-chem)

The open-source Community Earth System Model Version 2.2 (CESM2.2) is a modular software infrastructure that couples different components of the Earth System, i.e., the atmosphere, land and ocean (Danabasoglu et al., 2020). Based on the Community Atmosphere Model version 6 (CAM6), CAM-chem is the atmospheric component of the CESM2.2 with an interactive representation of physical, dynamical and chemical processes (Gettelman et al., 2019; Danabasoglu et al., 2020). The model has 32 vertical layers from the surface to around 40 km with a spatial resolution of 1.25° in longitude and 0.9° in latitude. Here we use the SLH chemistry presented in Fernandez et al. (2025) with the CH_4 emission-driven configuration described in Mirrezaei et al. (2025), which include updates to soil uptake of CH_4 and CO.

Table 1 lists the simulations conducted in this study. Our baseline simulation (CESM) uses the CMIP6 prescription of surface greenhouse gases (Meinshausen et al., 2017), extended with the Shared Socioeconomic Pathways 4-34 (SSP434) after 2015, with an alternative run (CESM-245) using the SSP245 to look at a different prescribed CH_4 distribution. The two scenarios do not differ widely for the considered period (2015-2023). Aside from the CESM-245 that is branched on January 1 2015 from the baseline simulation (CESM), all the simulations are initialized from a previous CAM-chem concentration-driven simulation's initial conditions on January 1 2002 and we use the year 2002 as the spin-up. All the CH_4 emission-driven simulations input posterior CH_4 fluxes from the NOAA CarbonTracker-CH4 2025 (CT-CH4-2025, Oh et al., 2025). For other chemical emissions, the CESM-CH4 uses the CAMS-GLOB-ANT_m1.1 (denoted hereafter as CAMS-MOSAIC) anthropogenic emission fluxes that has correction based on national inventory in Europe, USA and China with corrections at the state or province levels (Granier et al., 2025; Bouarar et al., 2026). However, surface CO anthropogenic fluxes are replaced with the posterior CO

https://doi.org/10.5194/egusphere-2026-4883
Preprint. Discussion started: 14 August 2026

emissions from Gaubert et al. (2024). In a previous study (Mirrezaei et al., 2025), we found that higher emissions in the NH were reducing OH biases and providing a better fit to CO and CH_4 observations. Wildfire emissions of chemical species other than CH_4 are prescribed from the Fire INventory from NCAR version 2.5 (Wiedinmyer et al., 2023), hereafter FINNv2.5. The CESM-CH4-CMIP7 uses the new set of emissions prepared for the phase 7 of the CMIP, which consists in Community Emissions Data System (CEDS) released on April 18 2025 (CEDS-CMIP-2025-04-18) for anthropogenic emissions (Hoesly et al., 2018; Feng et al., 2020; Hoesly et al., 2025) and the BB4CMIP7-2-1 fire emissions (van Marle and Werf, 2025). During our study period, the CMIP7 monthly wildfire emissions are derived from the Global Fire Emissions Database version 4.1s (Randerson et al., 2015; van Marle et al., 2017).

Figure 2 displays the emission time series estimated by the different datasets used in this study. With anthropogenic totals higher than 700 TgCO yr^{-1}, the posterior CO emissions are much larger than the CEDS-CMIP7, which ranges between 400 and 500 TgCO yr^{-1}. By construction, the posterior CO replicates the temporal variations from the prior CAMS-GLOB-ANT v5.3 inventory (Soulie et al., 2024), with no apparent trend globally. In contrast, the CEDS-CMIP7 show a reduction of around 20 %, which likely is closer to observational estimates of 14%–17% reduction (approximately 85–110 Tg yr^{-1}) from Tang et al. (2026). Because of the differences in anthropogenic emissions, we also perform another simulation with anthropogenic CO increased by 30 % for the entire period (CESM-CH4-CMIP7-CO). At every physical time step (30 min) and for all vertical levels, winds, temperature as well as specific humidity (Mirrezaei et al., 2025) are nudged to the MERRA-2 (Gelaro et al., 2017) using the 3-hourly outputs with a relaxation time of 12 hours (Davis et al., 2022). We also performed a couple of simulations with CMIP7 forcings (CESM-CH4-CMIP7-ERA5 and CESM-CH4-CMIP7-CO-ERA5) nudged to ERA5 hourly outputs (Hersbach et al., 2020). The ERA5 nudging is applied to the same variables and the same nudging strength as the MERRA-2.

In CESM, NMVOCs emissions from vegetation is estimated interactively in the Community Land Model (CLM) by the Model of Emission of Gases and Aerosols from Nature (MEGANv2.1), as initially described in Guenther et al. (2012). Thus, different atmospheric conditions can have strong impacts on biogenic emissions even though the phenology (parametrized by leaf area index) is prescribed by a climatology in our simulations. The monthly global isoprene emissions are reported on the Fig. 2 and show an offset between the two used reanalysis with a 2003-2022 average of 466 TgC yr^{-1} (MERRA-2) and 545 TgC yr^{-1} (ERA5). We found that the ERA5-nudged simulation is warmer over the tropical continents where isoprene emissions are higher (Fig. S1), suggesting that the temperature is driving emission change. Our isoprene emission estimates are higher than recent TROPOMI inversion (Sfendla et al., 2026) and of the CAMS-GLOB-BIOv3.1 dataset, who estimated isoprene emissions to be 389 TgC yr^{-1} for 2000-2019 (Sindelarova et al., 2022). However, it is well within the range of the most recent studies that derived isoprene emissions using Cross-track infrared sounder (CrIS) isoprene retrievals, with 456 $\pm$ 238 TgC yr^{-1} over 2013–2020 period (Li et al., 2025) and 628–711 Tg C yr^{-1} for 2019-2020 (Yoon et al., 2025).

2.2 Airborne Fields Campaigns Observations

We evaluate the simulations with four different field campaign observations. First, the High-Performance Instrumented Airborne Platform for Environmental Research (HIAPER) Pole-to-Pole Observations (HIPPO) aircraft campaigns (Wofsy, 2011)

https://doi.org/10.5194/egusphere-2026-4883
Preprint. Discussion started: 14 August 2026

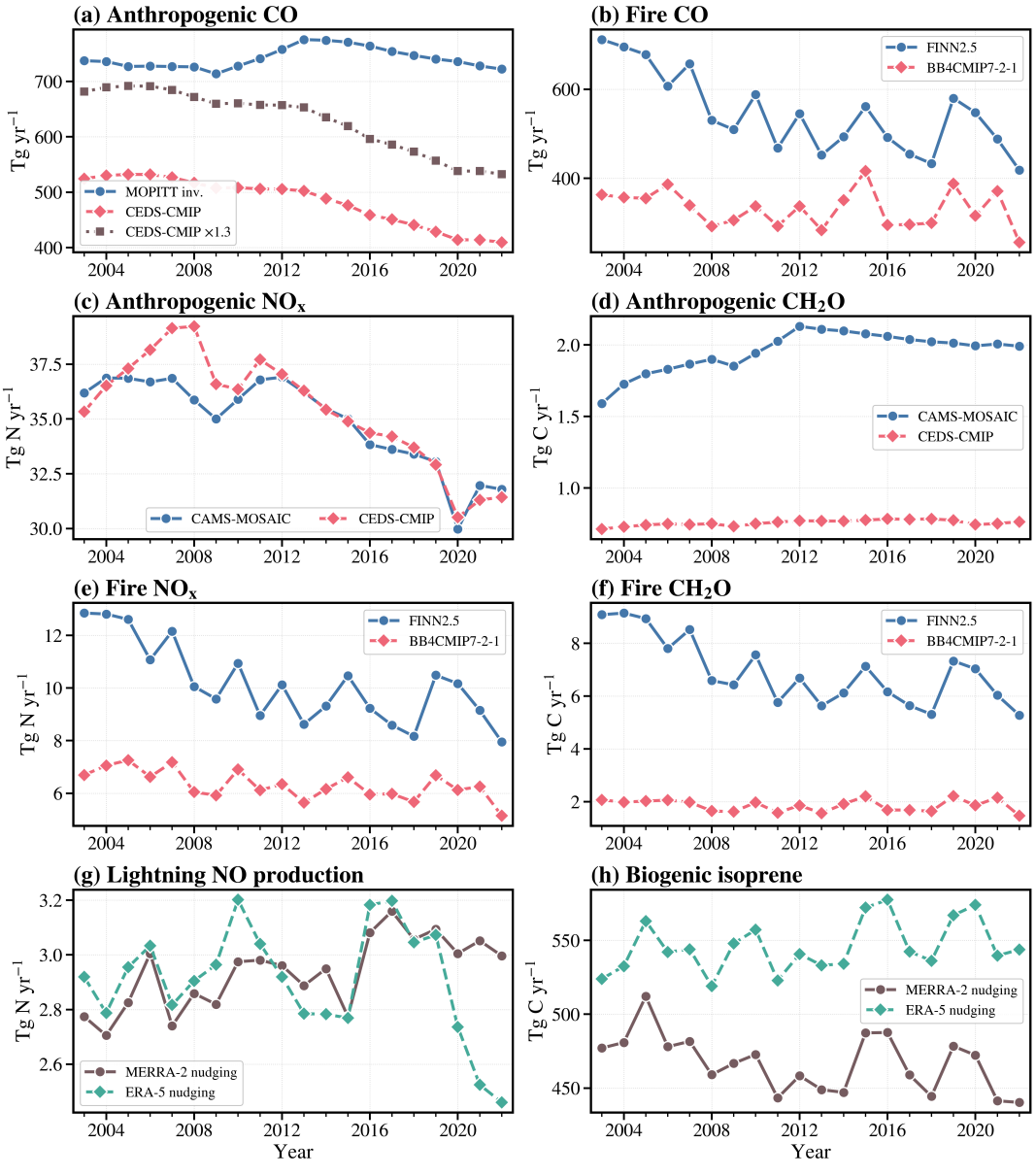

Figure 2. Global and annual emissions for A) Anthropogenic CO, B) Fire CO, C) Anthropogenic surface NO_x, D) Anthropogenic surface CH_2O, E) Fire surface NO_x, F) Fire surface HCHO, G) NO_x from lightning, F) Biogenic isoprene.

https://doi.org/10.5194/egusphere-2026-4883
Preprint. Discussion started: 14 August 2026

consisted of 5 deployment of the NSF/NCAR Gulfstream V aircraft (GV) in different seasons during the 2009–2011 period. The airborne vertical profiles provide CO and CH_4 in-situ measurements along the Pacific ocean between 87° N and 67° S (Santoni et al., 2014; Gaubert et al., 2019). Second, the NASA Atmospheric Tomography Mission (ATom) also provides a global survey of atmospheric composition with CO and CH_4 measured by the NOAA Picarro instrument (McKain and Sweeney, 2021). With hundreds of vertical profiles, ATom provides a global survey of the remote environment providing cross-sections along north-south gradients of the Atlantic and the Pacific ocean for 4 different deployments during the 2016-2018 period (Thompson et al., 2022). Third, we compare the results for O_3, CH_4 and CO with the Korea–United States Air Quality (KORUS-AQ) field study (Crawford et al., 2021). The KORUS-AQ experiment occurred in May and June 2016 and was characterized by high O_3 and CO pollution resulting from both local sources and long-range transport of East Asian sources (Miyazaki et al., 2019; Gaubert et al., 2020). Last, the Asian summer monsoon Chemical and Climate Impact Project (ACCLIP) occurred in August 2022 (Pan et al., 2024) and thus provide a snapshot of the conditions at the end of the study period. We use observations made aboard the NSF/NCAR GV which sampled a quite large area of the Western Pacific around South Korea and Japan, with flight durations of around 8 hours. All the the in-situ CO observations used in this study were calibrated on the WMO CO X2014A scale and the CH_4 measurements WMO CH4 X2004A standard.

2.3 NOAA Marine Boundary Layer Reference

We compared our simulations to the global and zonal means of CH_4 from NOAA Greenhouse Gas Marine Boundary Layer Reference (Lan et al., 2023) which derived from a subset of CH_4 measurements from air samples that are predominantly of well-mixed marine boundary layer (MBL) air with data smoothing and averaging approach from Masarie and Tans (1995). We linearly interpolate the 3-hourly model outputs in space and time to the observation locations and process the data same way as the MBL Reference.

2.4 Network for the Detection of Atmospheric Composition Change FTIR CO and CH_4 column retrievals

Ground-based Fourier Transform Infrared (FTIR) spectrometers operated within the Network for the Detection of Atmospheric Composition Change (NDACC) are used to further evaluate model simulations (De Mazière et al., 2018). The NDACC FTIR network spans a wide range of environments, from remote regions to sites influenced by urban emissions, providing broad geographic coverage for model evaluation. These instruments acquire direct-sun spectra under cloud-free conditions in selected mid-infrared spectral regions at a nominal spectral resolution of 0.004 cm^{-1}, enabling the retrieval of total columns and vertical information for CO, CH_4, and other atmospheric trace gases. NDACC FTIR observations are particularly well suited for investigating atmospheric variability and long-term trends. In this study, measurements from 21 NDACC sites were obtained from the NDACC archive (https://ndacc.larc.nasa.gov/) and daily mean total columns were calculated for dates coincident with the model simulations. The current analysis uses products generated with the retrieval strategies presently available in the archive. While these products are suitable for total-column comparisons, future analyses will incorporate updated retrievals that provide improved tropospheric and stratospheric information (Ortega et al., 2025). To ensure a consistent comparison,

https://doi.org/10.5194/egusphere-2026-4883
Preprint. Discussion started: 14 August 2026

modelled vertical profiles were smoothed using the FTIR averaging kernels and a priori profile, thereby accounting for the instrument's vertical sensitivity. The resulting smoothed model columns were then compared directly with the FTIR columns.

2.5 Measurements of Pollution in the Troposphere (MOPITT) CO column retrievals

The MOPITT instrument (Drummond et al., 2010) measures CO absorption bands in the near infrared (NIR, λ=2.7 μm) and the Thermal infrared (TIR, λ=4.7 μm). The version 9 (V9J) of the joint retrievals (Worden et al., 2010) estimates CO from both NIR and TIR and is described in Deeter et al. (2022). We use the level 3 product, which consists of monthly mean CO on a 1°x1° grid and are expressed here as column-averaged dry-air mole fraction. We apply the column forward operator to the regridded monthly model outputs.

2.6 Greenhouse Gases Observing Satellite (GOSAT) CH_4 column retrievals

We additionally evaluate the simulated column CH_4 against the University of Leicester GOSAT Proxy v9.0 product (Parker et al., 2020), retrieved from shortwave-infrared radiances measured by the JAXA Greenhouse Gases Observing Satellite (Kuze et al., 2009). Each Level-2 data, with its prior profile, pressure weights and column averaging kernel, is mapped to the CAM-chem grid ($0.9° \times 1.25°$). The simulated CH_4 is then interpolated onto the 20 retrieval levels and smoothed with the retrieval prior and averaging kernels following Appendix D of Parker and Boesch (2020).

2.7 TROpospheric Monitoring Instrument (TROPOMI) CO and CH_4 column retrievals

Flying on the ESA Copernicus Sentinel-5 Precursor platform, the TROPOMI instrument (Veefkind et al., 2012) is an imaging spectrometer passively measuring the reflected solar radiation, from which the column-averaged dry-air mole fraction of methane (XCH_4) can be estimated in the 1.65 μm band. For XCH_4 from TROPOMI we use the blended TROPOMI+GOSAT product of Balasus et al. (2023), in which the operational retrieval (Lorente et al., 2021) is recalibrated against GOSAT to remove albedo and aerosol related biases. The level-2 data are regridded to the CAM-chem resolution and the column averaging kernels are applied to the model profile. For CO, we use the Sentinel-5P TROPOMI CO total-column product (Borsdorff et al., 2018; Martínez-Alonso et al., 2020). We apply surface-dependent quality filtering, with only the highest-quality pixels over land ($\mathtt{qa} = 1.0$), and only pixels with $\mathtt{qa} \geq 0.7$ over ocean (excluding coastlines, lakes and inland water). Following Inness et al. (2022), the total-column averaging kernel is applied directly to the co-sampled model profile.

3 Results

3.1 Evaluation with Airborne Field Campaign Observations

Since the simulation results are quite consistent despite covering different regions and periods, we aggregate the comparison for the 4 different field campaigns in Figure 3. First, the CESM-SSP245 simulation, with prescribed CH_4 from observations before 2015 and SSP245 afterward, has a lowest CH_4 bias compared campaign observations from remote regions, i.e., HIPPO and

https://doi.org/10.5194/egusphere-2026-4883
Preprint. Discussion started: 14 August 2026

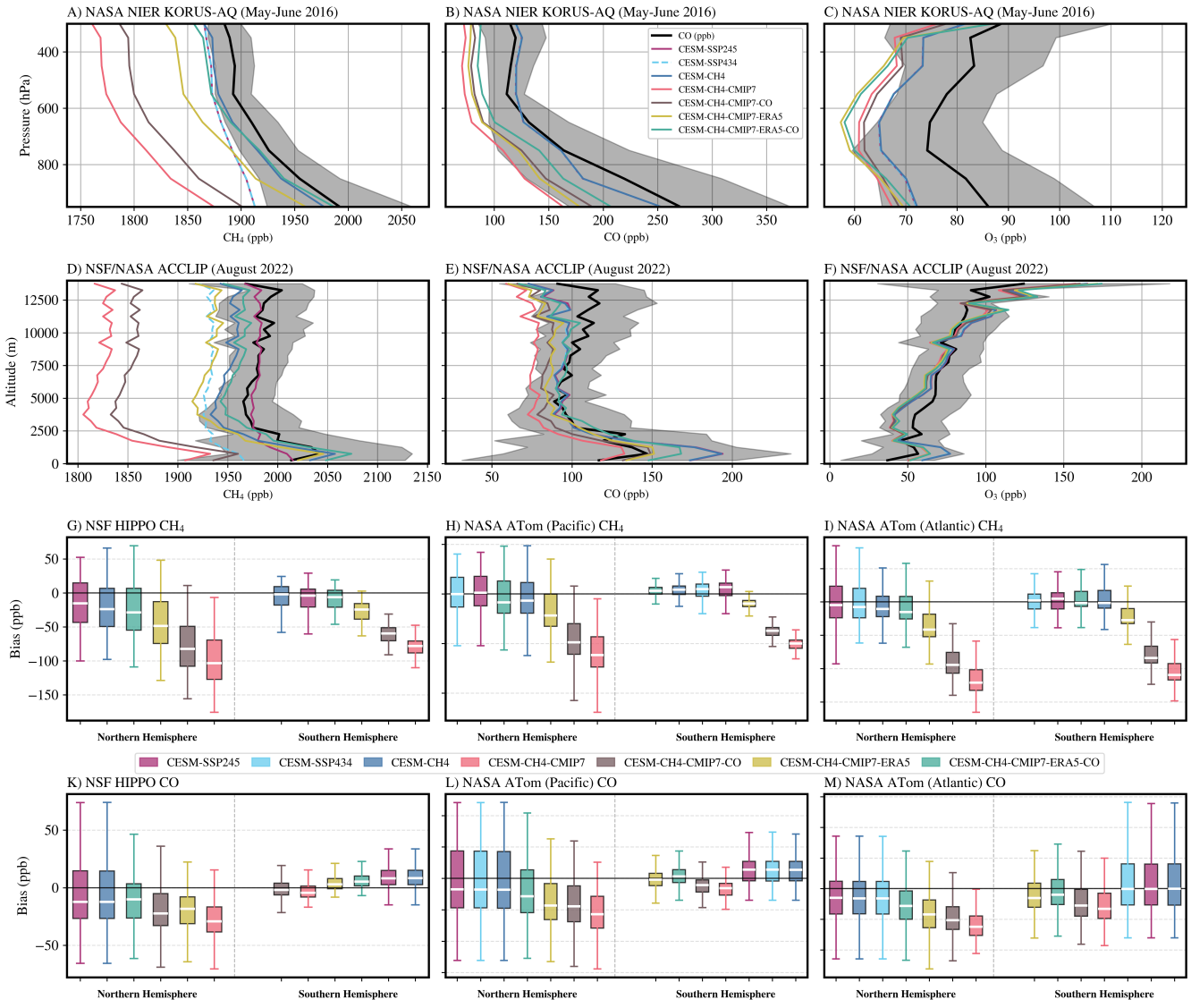

Figure 3. Comparison of simulation and observations of NIER/NASA KORUS-AQ for A) CH_4, B) CO and C) O_3 and with NSF/NASA ACCLIP for D) CH_4, E) CO and F) O_3. The grey area represents the observations standard deviation within each altitude bins (100 hPa for KORUS-AQ and 500 m for ACCLIP). The distribution of the bias for NSF HIPPO and NASA ATom are shown by hemisphere for CH_4 (G, H, I) and CO (K, L, M).

https://doi.org/10.5194/egusphere-2026-4883
Preprint. Discussion started: 14 August 2026

ATom. During KORUS-AQ and ACCLIP, these concentration-driven simulations have a lack of vertical variability in the model, resulting from the prescription of zonally averaged concentration fields that smearing the gradients in these regions where regional emissions dominate. The model shows a low CH_4 bias during KORUS-AQ with both CESM-SSP245 and CESM-SSP434, but not during ACCLIP where the CESM-SSP245 simulates CH_4 quite well. It is showing the difficulty of capturing the large temporal variations in CH_4 with the assumed emission/concentration projections in SSPs. Second, the CESM-CH4 simulation, with emission-driven CH_4, CAMS-MOSAIC, posterior CO, and FINN2.5 for chemical emissions provides better results for CH_4, CO and O_3, consistently across all field campaigns. The simulation has improved CH_4 vertical gradients and sometimes a lower bias than the prescribed CH_4 simulations. The boundary layer profile is correctly simulated by the CESM-CH4 simulation while the free tropospheric CH_4 is slightly underestimated, indicative of an overall OH overestimation, or an underestimation of the CH_4 sources during ACCLIP in summer 2022. Third, despite having the same CH_4 emissions, the set of simulations with emissions from CMIP7 (CESM-CH4-CMIP7 and CESM-CH4-CMIP7-CO) have a much lower CH_4 compared with the observations. The increase in CO (CESM-CH4-CMIP7-CO) only mitigates partially the CO underestimation and, through an OH reduction, the CH_4 low biases. Fourth, the simulations with nudging to ERA5 shows a much lower CH_4 and CO bias, indicative of a lower OH driven by meteorological differences (everything else being equal). The CESM-CH4-CMIP7-CO-ERA5 has a lower CH_4 underestimation and its profiles are closer to the CESM-CH4 simulation for both CH_4 and CO. This means the OH is lower in the CESM-CH4-CMIP7-CO-ERA5.

Regarding CO, the simulations using the posterior emissions overestimate the observations in the boundary layer around the Seoul Metropolitan Area during ACCLIP but the free tropospheric abundance is quite well simulated. Conversely, the CESM-CH4-CMIP7 with smaller CO emission is reproducing the boundary layer CO but underestimating the East-Asian background, probably because of a combination of an OH overestimation and/or an underestimation of the CO sources in East Asia. This might explain the O_3 overestimation in the boundary layer seen in CESM-CH4 but not in CESM-CH4-CMIP7.

Overall, this set of experiments shows that simulated CO tends to be underestimated in the NH in all the experiments with CMIP7 forcings. This could be the results of an indirect effect through a lack of NMVOCs emissions consuming OH and potentially producing CO in the atmosphere or the direct CO emission underestimation (that motivates our COX1.3 experiment), but it is likely a combination of both. However, as anthropogenic CO emissions are being reduced over the recent years, simulations with CMIP7 emissions provides a better CO during ACCLIP (summer 2022) than during KORUS-AQ (spring 2016), indicative of a better representation of the declining trends in CMIP7 than the posterior emissions derived from the weak trend of CAMS-GLOB-ANTv5.1. Finally, simulations run with the FINN2.5 emissions tends to overestimate CO in the southern hemisphere, related to the much higher estimate of fire CO emission compared to BB4CMIP7.

3.2 Evaluation against remote sensing observations

Figure 4 presents the summary comparison of simulated CO and CH_4 with TROPOMI, NDACC, GOSAT and MOPITT observations. The NDACC network has less coverage but higher spectral resolution and is used as reference for the given period (2010/01 to 2021/12 for GOSAT and 2018/05 to 2022/12 for TROPOMI). In line with the in-situ aircraft field campaign observations comparison, the remote sensing observations show that the CESM-CH4 and CESM-CH4-CMIP7-CO-ERA5 perform

https://doi.org/10.5194/egusphere-2026-4883
Preprint. Discussion started: 14 August 2026

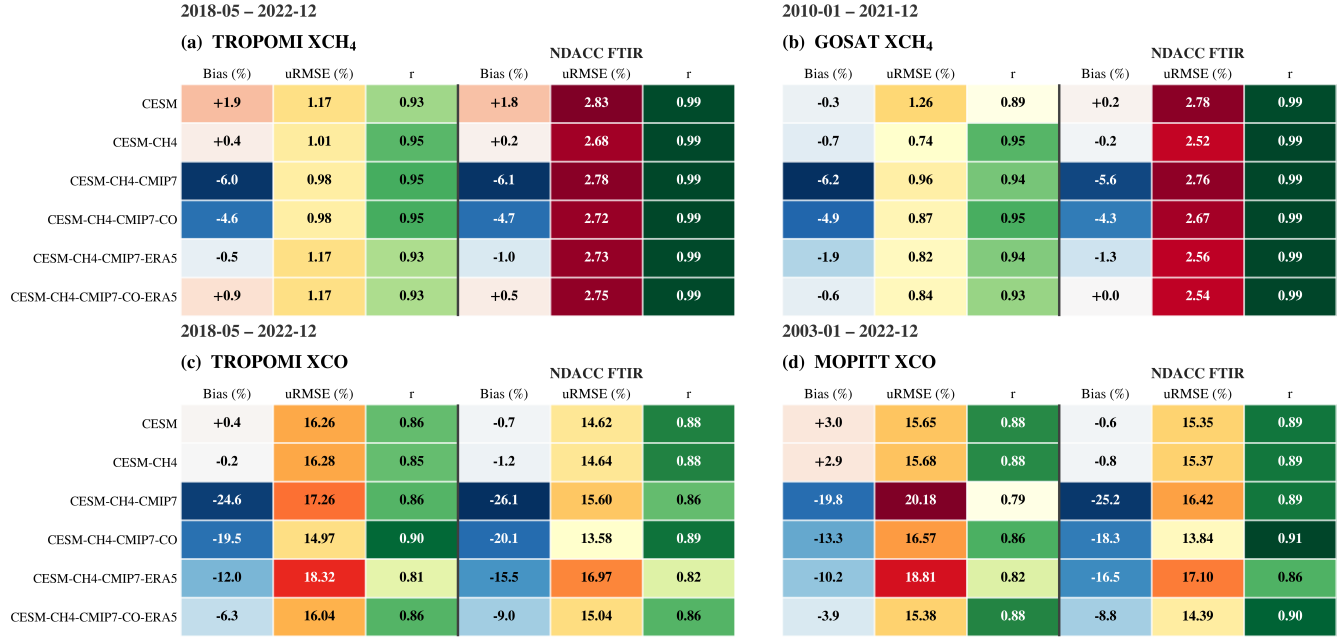

Figure 4. Comparison of simulation and observations for various periods and datasets: A) 2018/05–2022/12 TROPOMI XCH4 (n=1191664) and NDACC XCH4 (n=7237), B) 2010/01–2021/12 GOSAT XCH4 (n=801568) and NDACC XCH4 (n=19052), C) 2018/05–2022/12 TROPOMI XCO (n=2449501) and NDACC XCO, and D) 2003/01–2022/12 , MOPITT (n=12063679) and NDACC XCO (n=26921). The bias is shown on a diverging blue–white–red scale (blue where the model is lower than the observations, red where it is higher and white near zero), so colour shows both the sign and the magnitude of the bias. The unbiased RMSE (uRMSE) and the correlation coefficient r use sequential scales in which green marks the better value (low uRMSE, high r) and red/pale yellow the poorer value. Within each species (CH_4: A, B; CO: C, D), each metric (bias, uRMSE, and r) uses a single colour scale shared across both panels and across the satellite and NDACC FTIR blocks. For each observations, the systematic (bias) and random (uRMSE) uncertainty are estimated with correlation coefficient r.

best in simulating CH_4. These are the only two simulations with biases lower than 1 % for both GOSAT, TROPOMI, and NDACC for both periods. The CESM-CH4-CMIP7 and the CESM-CH4-CMIP7-CO have a systematic bias of around 4 to 6 % and indicate a reduction of up to 1 % in CH_4 low bias with an increase of anthropogenic CO by 30 %. Contrasting CESM-CH4-CMIP7-ERA5 and CESM-CH4-CMIP7 illustrate a change of around 5 % in CH_4 bias. The CESM-CH4-CMIP7-ERA5 has low biases as well, but underestimate CH_4 more during the GOSAT period. The random error (the unbiased RMSE, uRMSE) component does not vary as much as the systematic error across the experiments.

The relative uncertainties are higher for CO than for CH_4. Simulations that uses the posterior CO emissions estimated by Gaubert et al. (2024) have no biases on average with regards to TROPOMI, i.e., for the most recent period, and a small overestimation compared to MOPITT with errors of less than 3 %. Simulations with the setup following the CMIP7 protocols have a low CO compared to TROPOMI, MOPITT and NDACC observations, with up to a 25 % underestimation for CESM-

https://doi.org/10.5194/egusphere-2026-4883
Preprint. Discussion started: 14 August 2026

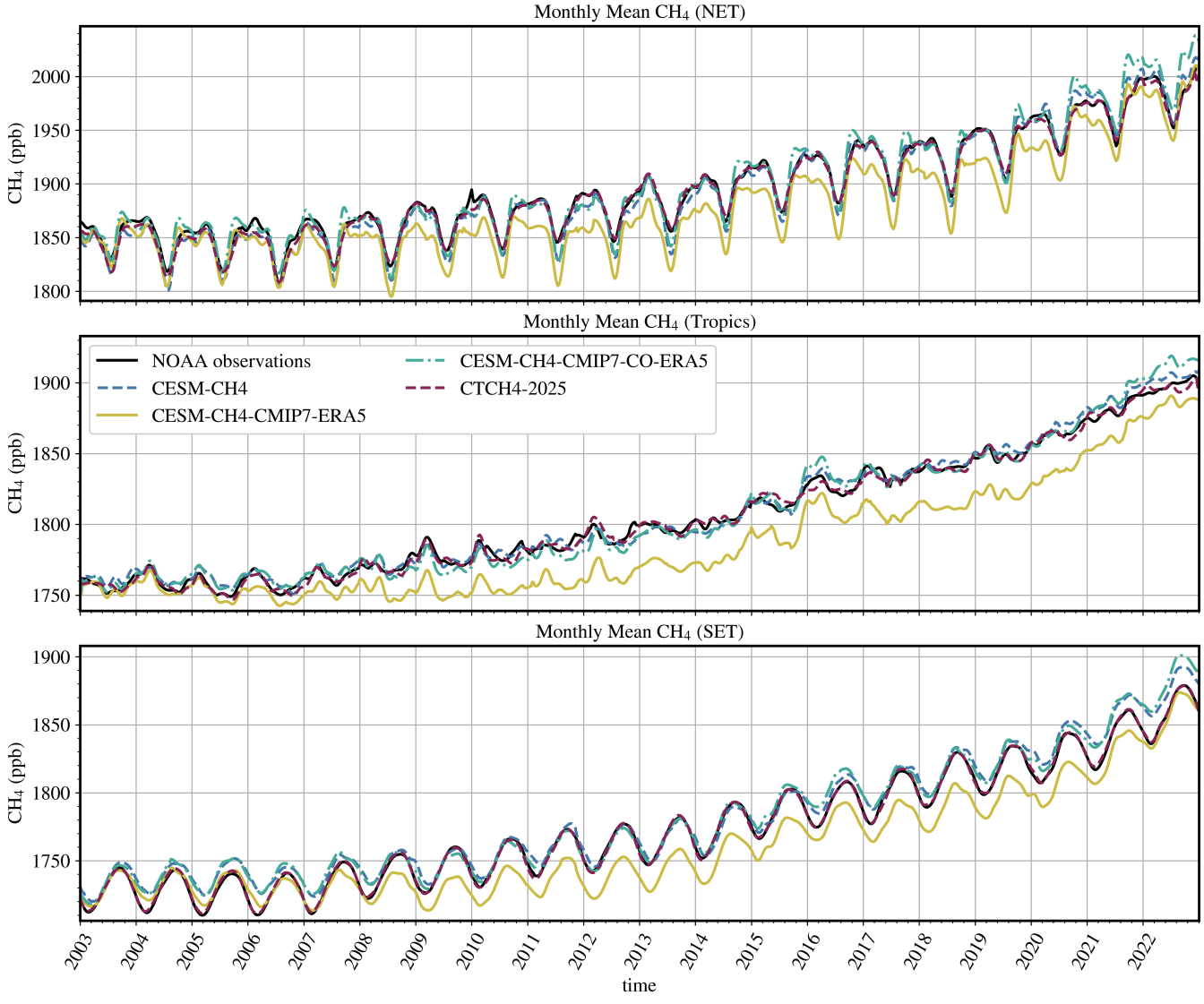

Figure 5. Comparison of simulation and observations of CH_4 with marine boundary layer sites average across zonal latitudinal bands, for Northern Hemisphere extratropics (NET; 30° N to 90° N), tropics (-17.5° N to 17.5° N), and the southern hemisphere extratropics (SET; -90° N to -30° N).

CH4-CMIP7. Increasing the anthropogenic CO emissions by 30 % reduces both the systematic and random errors, with around 5 % reduction in biases for all the observing systems. Consistent with the in-situ evaluation, replacing MERRA-2 with ERA5 substantially improved the performance of CESM-CH4-CMIP7-CO-ERA5 relative to CESM-CH4-CMIP7 simulation.

https://doi.org/10.5194/egusphere-2026-4883
Preprint. Discussion started: 14 August 2026

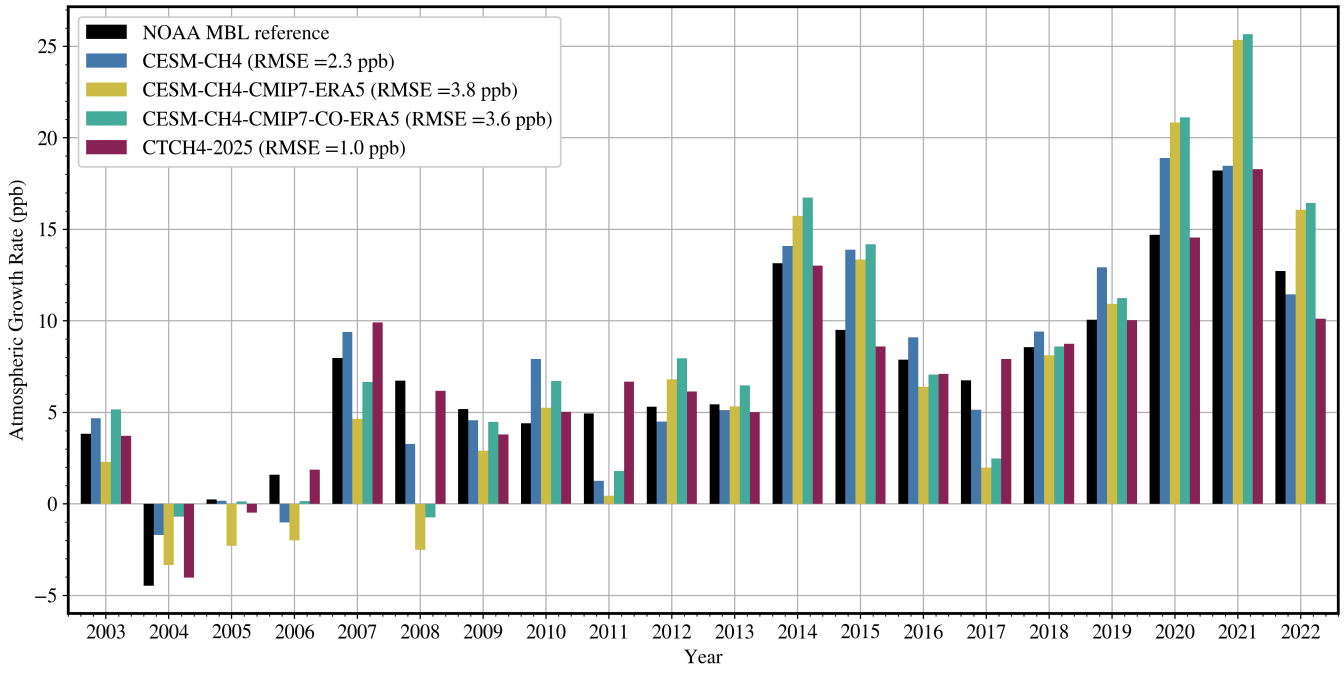

Figure 6. Annual CH_4 growth rate calculated using NOAA GML data extension and integration method.

3.3 NOAA Global Greenhouse Gas Reference Network

Figure 5 displays the zonally averaged NOAA marine boundary layer observations over three zonal bands. Based on the aforementioned comparison with four field campaigns, as well as GOSAT, NDACC, and TROPOMI CH_4 observations, we focus here on the three best-performing simulations: CESM-CH4, CESM-CH4-CMIP7-ERA5, and CESM-CH4-CMIP7-CO-ERA5. We added for reference the CT-CH4-2025, which assimilates the observations to estimate emissions using a different OH field and transport model (Oh et al., 2025). The effect of the OH overestimation is clearly illustrated for the CESM-CH4-CMIP7-ERA5 simulation where there is a major offset in CH_4 after 2007, especially for tropical regions. This low bias remains until the end of the simulation period. The CESM-CH4 and CESM-CH4-CMIP7-CO-ERA5 reproduce well the observations, including the long-term trends, interannual variability, and the seasonal cycles overall. It is only for some months where the simulated CH_4 is distinctively different in observations, with distinctive features in CESM-CH4 and CESM-CH4-CMIP7-CO-ERA5 because of monthly OH differences and potentially transport. These CH_4 disparities are larger and more frequent in the Northern Hemisphere extratropics.

Figure 6 shows the modelled annual growth rate estimated at NOAA Global Monitoring Laboratory's MBL sites. The same data extension and integration method is used for MBL reference and modelled trend and growth rate results, allowing Naturally, as a result of the assimilation of the observations, the CT-CH4-2025 has the best performance. However we note that differences can be higher than 1 ppb for a given year. Compared to CT-CH4-2025, our simulations have a different transport,

https://doi.org/10.5194/egusphere-2026-4883
Preprint. Discussion started: 14 August 2026

OH and soil uptake. The CESM-CH4 and CESM-CH4-CMIP7-CO-ERA5 reproduce well the growth rate, usually within the -3 to +3 ppb yr^{-1}, except for a larger overestimation in 2021. As these simulations are driven by CT-CH4-2025 CH_4 emissions, the overall dynamic of CH_4 growth rate is well simulated, with the pause for the years 2003 to 2006, a renewed growth after 2007, a decreasing growth from 2014 to 2017, followed by a renewed increase that peaks in 2021. Beside emissions, the chemical processes driving the variability of the CH_4 growth rate will be presented in the next sections. We will quantify the role of emissions and chemistry as well as investigate the processes driving the dynamics of the CH_4 growth rate in Sect. 5.

4 Comparison of simulation experiments

4.1 CH_4 budget

Table 2. CH_4 budget (2010-2019). The tropospheric chemical loss (L_{chem}) is calculated for all the reactions in the troposphere and for the CH_4+OH reaction in parenthesis. The chemical lifetime is the total atmospheric burden divided by the tropospheric sink, also with CH_4+OH reaction only in parenthesis. L_{dep} is the loss of CH_4 by soil uptake. All the units are $TgCH_4$ yr^{-1}, except for CH_4 lifetime in years. [a] Top-down range of the Global CH_4 Budget (Saunois et al., 2025). [b] Bottom-up estimates compiled by the Global CH_4 Budget (Saunois et al., 2025) [c] 2010 tropospheric CH_4 lifetime with regards to OH estimated by Prather et al. (2012) [d] Growth rate estimated from CH_4 observations from the Global Monitoring Laboratory (Lan et al., 2022) and converted to $TgCH_4$ yr^{-1} using a conversion factor of 2.77 $TgCH_4$ ppb^{-1} (Lan et al., 2021b; Nisbet et al., 2023).

Simulation	Source	L_{chem} (OH)	lifetime (OH)	L_{dep}	Growth rate
CESM	-	505 (491)	10.0 (10.2)	-	-
CESM-CH4	597	505 (491)	9.9 (10.2)	33.4	23.2
CESM-CH4-CMIP7	597	522 (507)	9.1 (9.4)	31.6	9.9
CESM-CH4-CMIP7-CO	597	519 (504)	9.3 (9.6)	32.1	12.2
CESM-CH4-CMIP7-ERA5	597	503 (486)	9.9 (10.2)	38.2	20.8
CESM-CH4-CMIP7-CO-ERA5	597	500 (482)	10.1 (10.5)	38.6	23.3
CESM-CH4-2003	563	497 (484)	9.9 (10.2)	32.6	-1.6
Literature estimates	575 [553–586][a]	569 - 563 [462–663][b]	- (11.2 ± 1.3)[c]	31 [11–49][b]	19.1 ± 2.1[d]

Table 2 show the CH_4 budget for the 2010-2019 period. The chemical lifetime is defined as the ratio of the global, whole-atmosphere CH_4 burden to the tropospheric loss (Saunois et al., 2025), and we also isolate the OH contribution to tropospheric loss. This quantity is conceptually distinct from the perturbation lifetime that describes how a pulse emission decays and is used in global warming potential calculations. The CH_4 chemical lifetime with respects to tropospheric OH varies between 9.4 and 10.5 years, which remains short in comparison to 11.2 ± 1.3 years from Prather et al. (2012). The estimated emissions

https://doi.org/10.5194/egusphere-2026-4883
Preprint. Discussion started: 14 August 2026

from the CT-CH4-2025 are on the higher end of the Global Methane Budget ensemble of top-down inversions (Saunois et al., 2025). The soil uptake matches the literature mean estimate that is slightly higher than 30 $TgCH_4$ yr^{-1}.

The CESM-CH4, CESM-CH4-CMIP7-ERA5 and CESM-CH4-CMIP7-CO-ERA5 chemical lifetime are well within the uncertainty range of the empirical estimate. As a result, the combination of slightly higher emissions and higher OH leads to an average growth rate that is close to the one derived by NOAA observations over the 2010-2019 period for the CESM-CH4, CESM-CH4-CMIP7-ERA5 and CESM-CH4-CMIP7-CO-ERA5. The range of tropospheric CH_4 loss to OH is between 480 and 490 $TgCH_4$ yr^{-1}, which is much lower than the values estimated by the suite of chemistry-climate models reported in Saunois et al. (2025). The emission-driven simulations with an OH overestimation thus underestimate the CH_4 atmospheric growth rate.

4.2 CO budget

Table 3. CO budget (2010–2019). P_{total} is the total chemical production. P_{CH_4} is the CO chemical production from CH_4 oxidation assuming a yield of 75 % (Gaubert et al., 2016). All units are Tg CO yr^{-1}, except chemical lifetime (days) and burden (Tg CO).

Simulation	Source	Anthro	Fire	Burden	P_{total}	P_{CH_4}	L_{chem}	L_{dep}	lifetime
CESM	1373	742	545	389	1533	640	2719	138	52.2
CESM-CH4	1373	742	545	389	1533	639	2719	138	52.2
CESM-CH4-CMIP7	918	484	332	297	1488	663	2276	97	47.7
CESM-CH4-CMIP7-CO	1061	629	332	320	1481	658	2397	109	48.8
CESM-CH4-CMIP7-ERA5	935	483	332	338	1588	630	2356	120	52.3
CESM-CH4-CMIP7-CO-ERA5	1078	629	332	362	1579	624	2742	134	53.6
CESM-CH4-2003	1373	742	545	386	1521	630	2710	138	52

The CO budget is displayed on Table 3. The average total direct emissions estimated from the sum of the posterior from Gaubert et al. (2024), FINN2.5, direct MEGAN CO, and a minor oceanic source amount to 1373 Tg CO yr^{-1}. This is much higher than 848 Tg CO yr^{-1} quantified by Tang et al. (2026), but only slightly higher than 1200 Tg CO yr^{-1} estimated by Zheng et al. (2019). Similarly, our total sources (Source + P_{total}) are 2906 Tg CO yr^{-1} in CESM-CH4 and 2657 Tg CO yr^{-1} in CESM-CH4-CMIP7-CO-ERA5, higher than 2395 Tg CO yr^{-1} from Tang et al. (2026) and 2,600 Tg CO yr^{-1} from Zheng et al. (2019). Despite different OH, biogenic emissions and CH_4, the CO chemical production does not change by a large amount when switching emission inventories. However using a different meteorological fields led to an additional CO chemical production (P_{total}) of 100 Tg CO yr^{-1}, which when combined with a different loss increased by 80 Tg CO yr^{-1}, led to a longer lifetime of 5 days, slightly less than a 10 % increase. The higher secondary CO results from higher biogenic emissions. The drivers of chemistry changes will be presented in the next section.

https://doi.org/10.5194/egusphere-2026-4883
Preprint. Discussion started: 14 August 2026

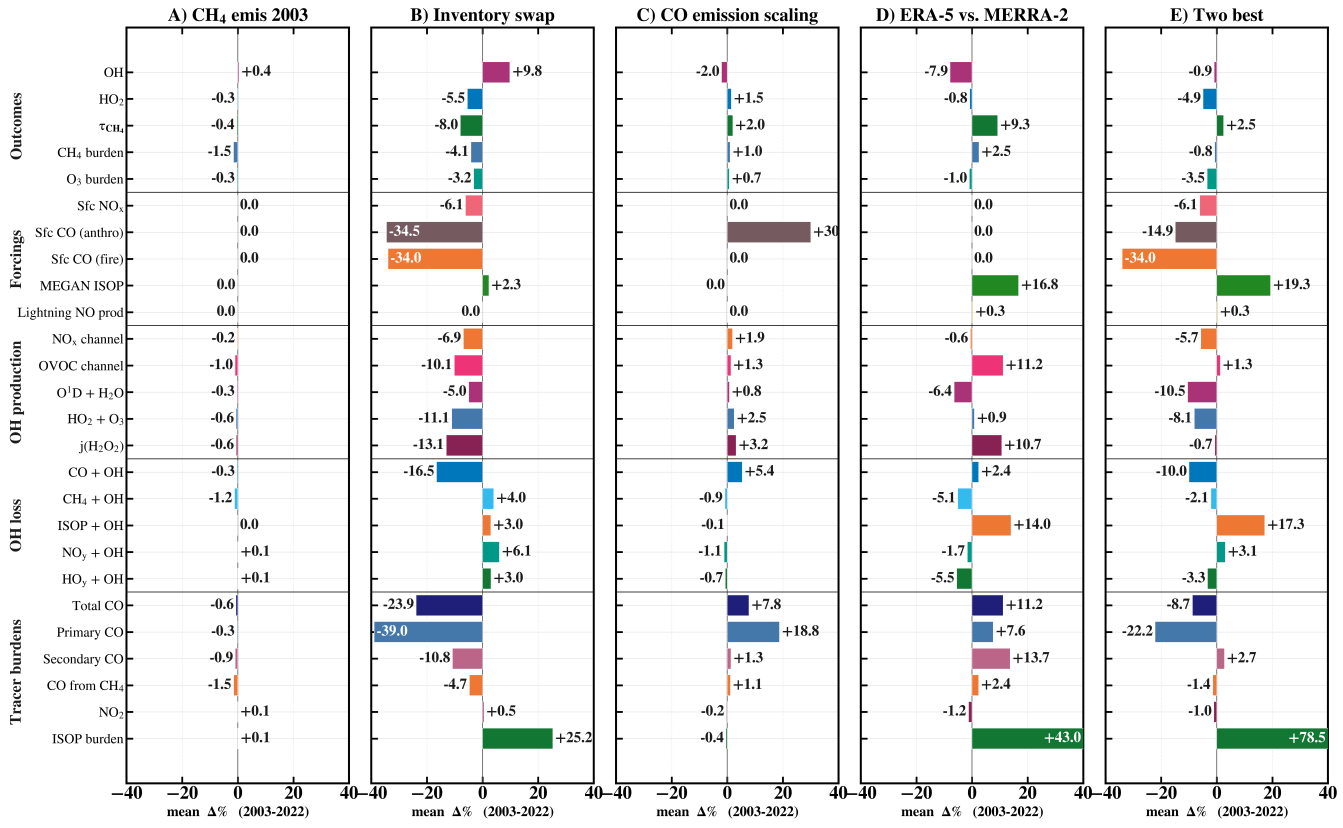

Figure 7. Differences in abundance for the various pair of experiments: A) CESM-CH4-2003 - CESM-CH4, B) CESM-CH4-CMIP7 - CESM-CH4, C) CESM-CH4-CMIP7-CO - CESM-CH4-CMIP7, D) CESM-CH4-CMIP7-CO-ERA5 - CESM-CH4-CMIP7-CO, E) CESM-CH4-CMIP7-CO-ERA5 - CESM-CH4

4.3 Drivers of chemistry changes

We investigate the impact of the model configurations and external forcings (i.e., CH_4 emissions, chemistry emissions, choice of meteorological reanalysis) on the OH budget and other related chemical fluxes. Figure 7 displays the changes in the OH sources and loss for various pairs of experiments. First, we contrast the changes if CH_4 emissions would have remained at 2003 levels (Figure 7A). This CH_4 emission scenario leads to a reduction in CH_4 burden by 1.5 %, reducing the OH loss, increasing OH burden, thus effectively shortening the CH_4 lifetime, and reduces O_3 formation, in line with previous studies (Prather et al., 2001; Fiore et al., 2002; Shindell et al., 2005). It directly reduces CO formation from CH_4 by 1.5 % and OH changes diminishes the CO lifetime. This reduced CO lifetime is illustrated by a lower primary CO despite the CO emissions being the same. Contrary to Staniaszek et al. (2022), both HO_2, O_3 and HO_2+O_3 reaction decrease following a CH_4 decrease. We also found a small reduction in other channels of OH production that are not related to O_3, the NO_x, oxygenated VOCs (OVOCs) and the H_2O_2 photolysis, some of which might be related to the reduction in products of the CH_4 oxidation.

https://doi.org/10.5194/egusphere-2026-4883
Preprint. Discussion started: 14 August 2026

Second, we look at the impact of changing anthropogenic and fire emission inventories of non CH_4 species (Figure 7B), as described on the Fig. 2. In the CESM-CH4-CMIP7, emissions of NO_x, CO and of most NMVOCs are lower. The reduction in fire and anthropogenic sources of CO, combined with a lower secondary CO leads to a net 16.5 % reduction in OH loss due to CO, which seems to be a dominant driver of the OH increase. However, the net change in NMVOCs, CO and NO_x appears to reduce O_3 and HO_2, thus lowering the OH source. Despite having the same nudging in both cases, the isoprene emissions are 2.3 % higher, likely due to reduced aerosol emissions from fires (Fig. 2) interacting with radiation. Fig. S2 shows that the CESM-CH4-CMIP7 - CESM-CH4 isoprene difference is small compared with the meteorology-driven change (Fig. S1). The lower NO_x emissions directly reduce the OH chemical production through NO_x recycling source. This only partly mitigates the OH increase from the inventory change, the net impact of emission change is an OH increase.

Third, we examine a 30 % perturbation of CO emission (Fig. 7C). The results are in line with Gaubert et al. (2016), where the primary impacts of CO increase is an OH reduction, which decreases the other OH losses and thus effectively increases CH_4 lifetime. Also, the secondary feedback is an increase in O_3, in the presence of NO_x and H_2O_2, more efficiently recycling OH and reducing the impact of the perturbation.

Fourth, we analysed the impact of meteorology, by contrasting a nudging to ERA5 and MERRA-2 reanalysis (Fig. 7D). We found that the simulation with ERA5 has 7.9 % less OH than the one driven from MERRA-2, resulting in a 9.3 % longer CH_4 lifetime and 2.5 % increase in burden. This result is consistent with differences in global annual mean OH levels driven by meteorological forcings (Gaubert et al., 2017; He et al., 2021). The main driver is the large increase of MEGAN isoprene emissions by +16.8 % (Fig. 2), driven by higher temperatures in the ERA5 nudged simulation (Fig S1). This leads to a higher isoprene burden (+43 %) and isoprene+OH loss (+14 %). The latter led to a larger secondary CO source (+13.7 %) and subsequent CO+OH loss (+2.4 %). While there is a net increase in the OVOCs and H_2O_2 sources of OH, there is also a net decrease in O_3 and thus primary OH formation (-6.4 %). The meteorology also led to a net reduction in OH loss through radical–radical reactions (-5.5 %). Clearly, the impact of emissions from vegetation simulated by MEGAN is the main process behind the large changes in the oxidative power of the atmosphere with around 8 % change in CH_4 lifetime. Finally, the comparison between the 2 best experiments: CESM-CH4-CMIP7-CO-ERA5 and CESM-CH4, reflects the combined effect of the chemical emissions although with the impact of CO scaling, and meteorology previously described, with notable cancellation of CO and isoprene emissions.

4.4 OH budget

Lelieveld et al. (2002) assessed the role of the O_3 photolysis source of OH as primary production (P) as opposed to radical driven OH formation (secondary, S) and introduced the concept of OH recycling probability r, defined as 1 - P/G, with P/G the ratio of the primary to the total gross production G, in Tmol $year^{-1}$. For higher OH recycling probability, with r values larger than 0.5, the tropospheric chemistry system is not as dependent on changes in ozone and other parameters related to primary production. It is also more resilient to CH_4 and CO perturbations. Figure 8 displays the OH budget and include both the total burden in moles and the relative contribution of each reaction. We follow the family defined in Lelieveld et al. (2016) and display their budget estimate for the year 2013. Bossolasco et al. (2025) provided a comprehensive evaluation of the impact

https://doi.org/10.5194/egusphere-2026-4883
Preprint. Discussion started: 14 August 2026

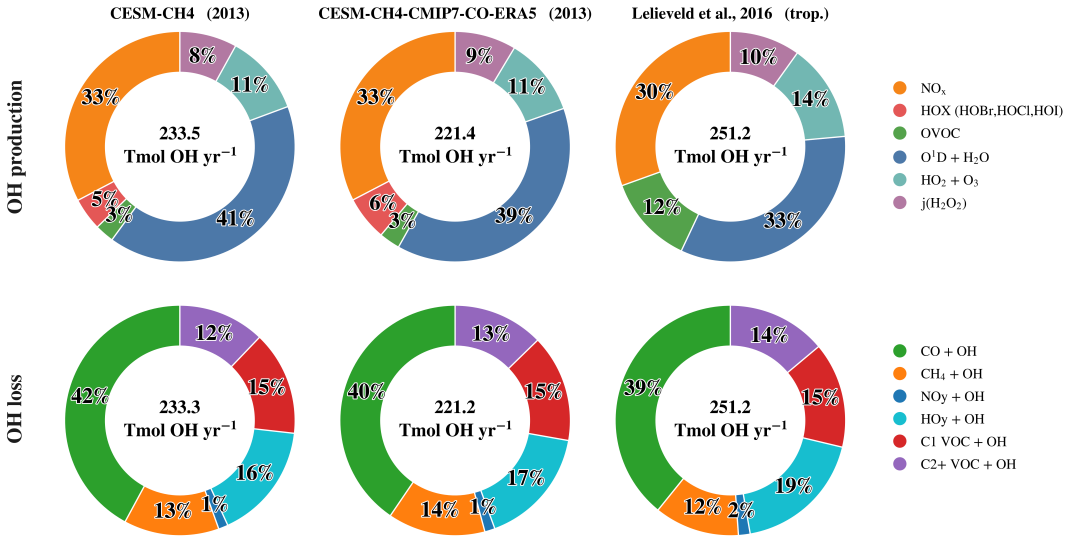

Figure 8. OH budget for the year 2013 by source (first row) and loss (second row) in Tmol year^{-1} with the contribution of each family defined in Lelieveld et al. (2016).

of the inclusion of SLH representation in CESM1 and estimated a value for r of nearly 60 %, indicative of naturally resilient atmospheric oxidising capacity. We found that the relative (%) contribution of each OH production's pathway remains fairly consistent with Bossolasco et al. (2025), i.e., between CESM1 and CESM2. Our results are in line with their findings of r being around 60 %. Our relative and absolute contribution of the additional source of OH through halogen photolysis is also consistent. However, their estimate for the OH budget for climatological year 2000 is 173.7 Tmol year^{-1}, which is much smaller than our estimates between 220 and 234 Tmol year^{-1} for the year 2013. Using CESM-CH4 as reference, the OH production is fuelled by higher primary OH formation, NO_x and O_3 + HO_2 recycling, and H_2O_2 photolysis. This could be driven by the addition of OVOCs in the MOZART-T1 mechanism (Emmons et al., 2020), differences in emissions, and overall model structural differences.

Lelieveld et al. (2016) used the Mainz Organics Mechanism (MOM) and included a significantly larger number of species, of the order of several hundreds. While their range of isoprene emissions (546–578 TgC yr^{-1}) is only slightly higher than our model simulations (on average 545 TgC yr^{-1} when driven by ERA5), they found a much higher source of OH from OVOCs, corresponding to 12 % of the OH source as opposed to 3 % in our model's chemistry. The higher OH source explains the higher OH burden although it is partially balanced by higher OH loss through VOC and CO reaction with OH. Their relative family contributions are similar to our simulations. It also raises the role of VOC oxidation playing, both as a source and a sink to OH. A lack of CO chemical formation could explain some of the CO and CH_4 underestimation without having the need to increase CO anthropogenic or fire emission to match the observations. This reinforces the need to integrate complex chemistry mechanisms to fully understand the OH budget, integral to the quantification of the variation in CH_4 oxidation.

https://doi.org/10.5194/egusphere-2026-4883
Preprint. Discussion started: 14 August 2026

5 Decomposition of the drivers of the CH_4 Atmospheric Growth Rate

Figure 9 links the simulated CH_4 growth-rate variability to the simulated evolution of tropospheric OH in the two best-performing configurations. Panel (a) shows annual OH anomalies (relative to the 2003–2022 mean) together with the ENSO phase, while panels (b,c) decompose the year-to-year change in the CH_4 growth rate (ΔGR) into its individual budget terms and compare the simulated changes with the NOAA record. The blue bars isolate the oxidation contribution, $-m\,\Delta k$, allowing the role of OH variability to be distinguished from that of emissions. Following Qu et al. (2022) the decomposition of the CH_4 growth rate changes is defined as:

$$\frac{\mathrm{d}^2 m}{\mathrm{d}t^2} = \frac{\mathrm{d}E}{\mathrm{d}t} - m\frac{\mathrm{d}k}{\mathrm{d}t} - k\frac{\mathrm{d}m}{\mathrm{d}t} - \frac{\mathrm{d}L}{\mathrm{d}t} \tag{1}$$

where m is the atmospheric CH_4 burden, E the emissions, k the OH loss frequency, and L the non-OH sinks. Accordingly, each change in CH_4 growth rate is the annual sum of an emission term (ΔE), an OH-driven oxidation term ($-m\,\Delta k$), a first-order relaxation term ($-k\,\Delta m$), and changes in non-OH sinks ($-\Delta L$). The value plotted for year t represents the change from the previous year ($t-1$) to the current year (t). For Δk and Δm, the value is evaluated as the differences between December–January mean burden, and m is the mass at the beginning of the studied year, calculated from the December–January mean as well. These four contributions are listed beneath each panel in Figure 9 and reproduce ΔGR. The bottom row gives the ratio $|-m\,\Delta k|/|\Delta E|$, which measures the relative importance of oxidation and CH_4 emission forcing and it is undefined in years when $\Delta E \approx 0$. This attribution follows Qu et al. (2022), which Chen et al. (2025) identified as the preferred approach because it partitions the two physical forcing terms (ΔE and $-m\,\Delta k$) while preserving budget closure. Because both experiments use identical CT-CH_4-2025 surface CH_4 emissions, ΔE is identical between them, as are the comparatively small $-k\,\Delta m$ and $-\Delta L$ terms. Consequently, differences between the two simulations arise almost entirely from their different representations of OH variability.

Panel (a) provides the physical interpretation of the decomposition. Tropospheric OH generally follows the expected ENSO response, with enhanced OH during La Niña and reduced OH during El Niño. Because the oxidation contribution depends on the year-to-year change in OH rather than its absolute magnitude, the slope of the OH time series determines the sign of the blue bars: increasing OH strengthens CH_4 oxidation and lowers the growth rate ($-m\,\Delta k < 0$), whereas decreasing OH weakens oxidation and increases CH_4 growth. Overall, emissions determine most of the large interannual growth-rate anomalies, while OH variability acts primarily as a modulator that either amplifies or offsets the emission-driven tendency. Only during periods of rapid and strong OH adjustment does oxidation become the dominant forcing. The remaining budget terms are comparatively small. The relaxation term $-k\,\Delta m$ is consistently negative and gradually increases in magnitude from nearly zero in the early 2000s to about -0.8 and -2.5 ppb yr^{-1} in 2020–2022, reflecting the growing atmospheric CH_4 burden. By contrast, changes in soil uptake remain negligible throughout the record ($|\Delta L| < 0.5$ ppb yr^{-1}), confirming that interannual variability is controlled almost entirely by OH chemistry. Most years are clearly emission dominated. During the beginning period, for example, the sharp decline in CH_4 growth in 2004 (ΔGR$= -9.1$ and -10.0 ppb yr^{-1} in CESM-CH4 and CESM-CH4-CMIP7-CO-ERA5, respectively) agrees closely with the observed decrease and is primarily driven by reduced emissions ($\Delta E = -6.8$ ppb yr^{-1}), while increasing OH provides an additional negative contribution ($-m\,\Delta k = -2.2$ and -2.7 ppb yr^{-1}). Likewise, the large

https://doi.org/10.5194/egusphere-2026-4883
Preprint. Discussion started: 14 August 2026

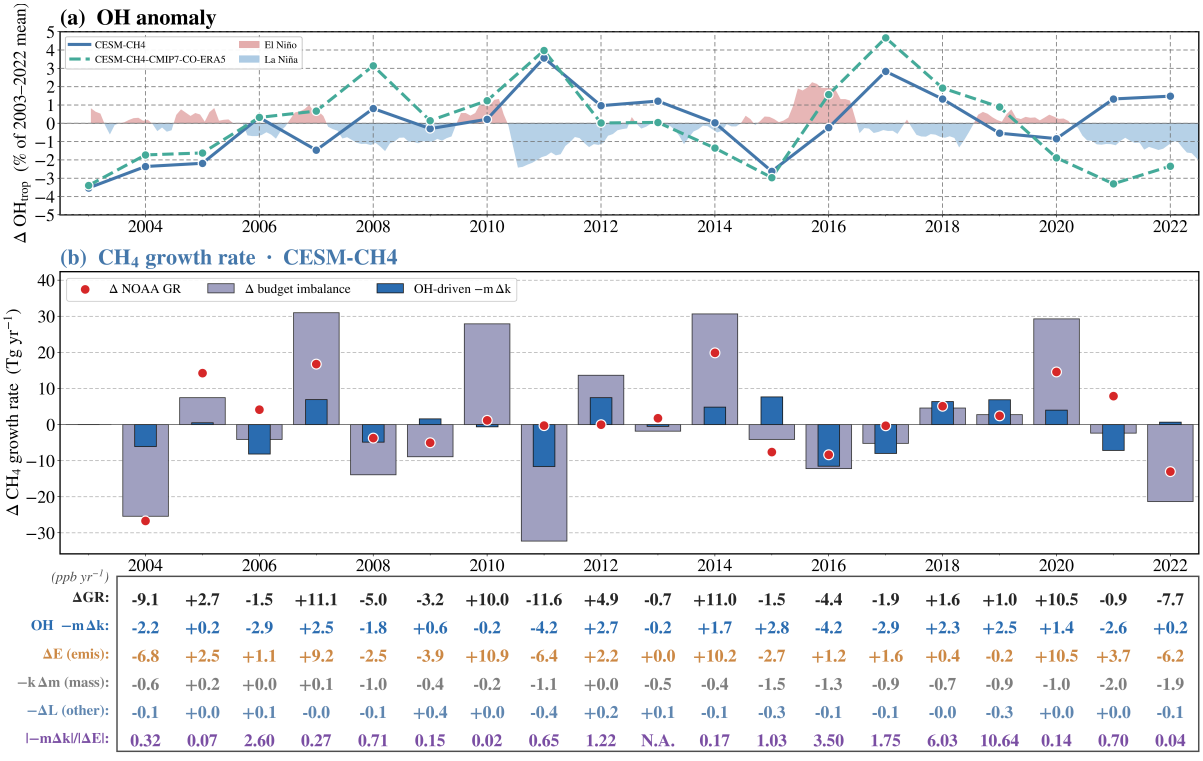

(ppb yr^{-1})	2004	2005	2006	2007	2008	2009	2010	2011	2012	2013	2014	2015	2016	2017	2018	2019	2020	2021	2022
ΔGR:	-9.1	+2.7	-1.5	+11.1	-5.0	-3.2	+10.0	-11.6	+4.9	-0.7	+11.0	-1.5	-4.4	-1.9	+1.6	+1.0	+10.5	-0.9	-7.7
OH −mΔk:	-2.2	+0.2	-2.9	+2.5	-1.8	+0.6	-0.2	-4.2	+2.7	-0.2	+1.7	+2.8	-4.2	-2.9	+2.3	+2.5	+1.4	-2.6	+0.2
ΔE (emis):	-6.8	+2.5	+1.1	+9.2	-2.5	-3.9	+10.9	-6.4	+2.2	+0.0	+10.2	-2.7	+1.2	+1.6	+0.4	-0.2	+10.5	+3.7	-6.2
−kΔm (mass):	-0.6	+0.2	+0.0	+0.1	-1.0	-0.4	-0.2	-1.1	+0.0	-0.5	-0.4	-1.5	-1.3	-0.9	-0.7	-0.9	-1.0	-2.0	-1.9
−ΔL (other):	-0.1	+0.0	+0.1	-0.0	-0.1	+0.4	+0.0	-0.4	+0.2	+0.1	-0.1	-0.3	-0.1	-0.1	-0.0	-0.3	+0.0	+0.0	-0.1
|−mΔk|/|ΔE|:	0.32	0.07	2.60	0.27	0.71	0.15	0.02	0.65	1.22	N.A.	0.17	1.03	3.50	1.75	6.03	10.64	0.14	0.70	0.04

(ppb yr^{-1})	2004	2005	2006	2007	2008	2009	2010	2011	2012	2013	2014	2015	2016	2017	2018	2019	2020	2021	2022
ΔGR:	-10.0	+2.2	-1.3	+7.8	-5.9	+0.1	+9.2	-10.5	+7.0	-0.7	+11.0	-3.0	-7.6	-1.9	+3.6	-0.6	+14.0	+4.8	-9.7
OH −mΔk:	-2.7	-0.0	-2.5	-0.7	-2.9	+3.8	-1.1	-3.3	+4.9	-0.0	+1.9	+1.1	-7.1	-3.3	+4.2	+0.8	+4.8	+3.2	-0.9
ΔE (emis):	-6.8	+2.5	+1.1	+9.2	-2.5	-3.9	+10.9	-6.4	+2.2	+0.0	+10.2	-2.7	+1.2	+1.6	+0.4	-0.2	+10.5	+3.7	-6.2
−kΔm (mass):	-0.8	+0.1	-0.1	+0.0	-0.7	-0.1	-0.2	-1.0	-0.0	-0.7	-0.6	-1.7	-1.4	-0.7	-0.5	-0.8	-0.8	-2.1	-2.5
−ΔL (other):	-0.3	-0.2	+0.0	-0.3	-0.1	+0.3	+0.0	-0.3	+0.2	+0.1	-0.1	-0.0	-0.3	-0.0	-0.1	-0.4	-0.1	+0.2	-0.3
|−mΔk|/|ΔE|:	0.39	0.01	2.24	0.07	1.16	0.97	0.10	0.51	2.25	N.A.	0.19	0.41	6.03	1.99	11.09	3.58	0.46	0.89	0.15

Figure 9. Inter-annual OH anomaly and its contribution to the CH_4 growth rate. (a) OH anomaly (per cent of the 2003–2022 record mean) for CESM-CH4 and CESM-CH4-CMIP7-CO-ERA5, with ENSO phases shaded. (b, c) Year-to-year change in the CH_4 growth rate: ΔGR (grey bars), the change in the NOAA rate (red points) and the OH-driven term $-m\,\Delta k$ (blue bars). The table lists $\Delta\mathrm{GR} = \Delta E - m\,\Delta k - k\,\Delta m - \Delta L$ (ppb yr^{-1}) and the ratio $|-m\,\Delta k|/|\Delta E|$.

https://doi.org/10.5194/egusphere-2026-4883
Preprint. Discussion started: 14 August 2026

positive growth-rate anomalies in 2010 and 2014 arise almost entirely from enhanced emissions ($\Delta E \approx 10$–11 ppb yr^{-1}), with oxidation playing only a minor role ($|-m\Delta k|/|\Delta E| < 0.2$ in 2014). The clearest examples of oxidation-dominated variability coincide with major ENSO transitions. During the 2010–2012 La Niña, OH increased rapidly to its highest value of the record, producing strong negative oxidation anomalies in 2011 (-4.2 and -3.3 ppb yr^{-1}). As OH relaxed during 2012, the oxidation contribution became positive. The opposite behaviour occurs during the 2015–2016 El Niño. OH reaches a minimum in 2015 before increasing rapidly into the 2017 maximum, making 2016 the most OH-dominated year of the record, with oxidation contributions of -4.2 and -7.1 ppb yr^{-1} and forcing ratios of 3.5 and 6.0 in the two simulations. Apart from a few years with very small growth-rate changes (2006, 2013 and 2019), both simulations reproduce the same overall relationship between ENSO, OH variability and CH_4 growth. The most informative period is the 2020–2022 triple La Niña because it departs from the canonical ENSO–OH relationship. In CESM-CH4, OH increases as expected during La Niña, producing a negative oxidation contribution that largely offsets the emission increase and keeps the simulated CH_4 growth rate close to the NOAA observations. In contrast, CESM-CH4-CMIP7-CO-ERA5 simulates a continued decline in OH despite persistent La Niña conditions. The resulting positive oxidation contribution reinforces the emission-driven increase, leading to a systematic overestimate of the observed CH_4 growth. For the single year 2020, the OH-driven forcing is $+1.4$ ppb yr^{-1} (≈ 4 Tg a^{-1}) in CESM-CH4 and $+4.8$ ppb yr^{-1} (≈ 13 Tg a^{-1}) in CESM-CH4-CMIP7-CO-ERA5, corresponding to about 12 % and 31 % of the combined emission-plus-OH forcing ($\Delta E - m\,\Delta k$). The CESM-CH4 value is close to the 5 Tg a^{-1} (14 %) that Qu et al. (2022) attribute to the 2019–2020 OH decline, whereas the ERA5 configuration roughly doubles this contribution, consistent with its overly strong meteorology-driven OH decline noted above. Integrated over 2020–2022, the cumulative OH contribution is close to zero in CESM-CH4 but approximately +7 ppb yr^{-1} in CESM-CH4-CMIP7-CO-ERA5, indicating that uncertainty in meteorologically driven OH variability alone can account for roughly one-fifth of the simulated CH_4-growth anomaly. Over the surge, CESM-CH4-CMIP7-CO-ERA5 overshoots the NOAA growth rate while CESM-CH4 stays close to it (Fig. 6), suggesting that ERA5 and CMIP7-emission driven OH decline is too strong, or that the prescribed OH assumed in deriving the CT-CH4-2025 emissions is too high. Splitting the difference between the two experiments (Fig. S7) into an emission change under the same meteorology (CESM-CH4-CMIP7-CO − CESM-CH4) and a switch of the reanalysis nudging field (CESM-CH4-CMIP7-CO-ERA5 − CESM-CH4-CMIP7-CO) shows that meteorology dominates in 2020–2022 and in the early 2000s, whereas anthropogenic and fire emissions matter more in 2016–2019. Consistent with this, Fig. 2 shows that lightning emissions under ERA5 are often higher, but lower during 2020–2022. Their spatial patterns are shown in Fig. S3.

6 Attributing the OH budget changes to their drivers over time

The growth-rate decomposition of Section 5 and Figure 9 attributes a variable part of the CH_4 growth rate to the inter-annual OH anomaly. Here we explain that anomaly. Figure 10 shows the temporal change of OH budget terms with the deseasonalised annual anomaly of every reaction channel. The result reflects the most important drivers of the OH budget outlined in a previous section, with NO_x and O_3 being the main source and CO being the main loss. Interestingly, the importance of the buffering

https://doi.org/10.5194/egusphere-2026-4883
Preprint. Discussion started: 14 August 2026

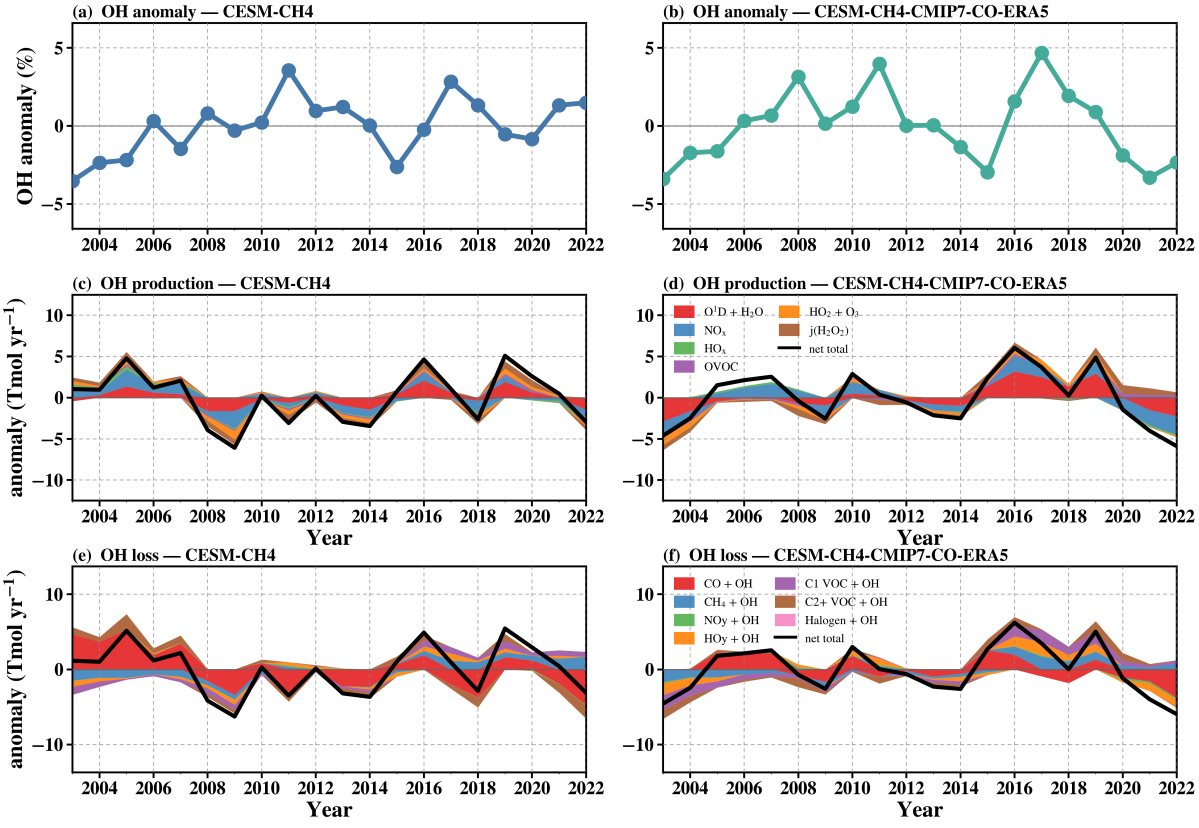

Figure 10. Tropospheric OH budget over 2003–2022 by reaction channel (detrended annual anomalies), for CESM-CH4 (left) and CESM-CH4-CMIP7-CO-ERA5 (right). (a, b) OH anomaly (%), (c, d) production and (e, f) loss channels (Tmol yr^{-1}), stacked about zero with the net as the black line.

effect is highlighted by the fact that higher variability in chemical fluxes do not always lead to higher OH anomalies, and the highest OH anomalies do not necessarily correspond to strong chemical flux anomalies.

To further understand these temporal changes, we perform a regression of the OH anomalies on its drivers. The regression is carried out by region and aggregated globally by weighting each region by CH_4+OH loss following Lawrence et al. (2001), so that the attribution reflects the oxidizing capacity that controls CH_4 removal. The weighting, and its robustness to alternative choices (air mass and OH burden), is detailed in supplementary texts S1–S2 and Fig. S8. The first regression is against forcings (surface NO_x, anthropogenic and fire CO, sector-tagged CH_4 emissions) and meteorological/chemical terms: lightning NO, the $O_3 \rightarrow O(^1D)$ photolysis frequency $J(O_3)$ and water vapour (Fig. 11). The second is based on reactant abundances such as CO, NO_2, O_3, isoprene and CH_4 (Fig. 12). The two bases reconstruct ≈ 69 % and ≈ 92 % of the global OH variance for CESM-CH4-CMIP7-CO-ERA5, and ≈ 63 % and ≈ 87 % for CESM-CH4 (Fig. S9), and the CH_4 emissions are negligible throughout, so the inter-annual OH signal is set mainly by NO_x, CO and ozone photochemistry rather than by the CH_4 fluxes.

https://doi.org/10.5194/egusphere-2026-4883
Preprint. Discussion started: 14 August 2026

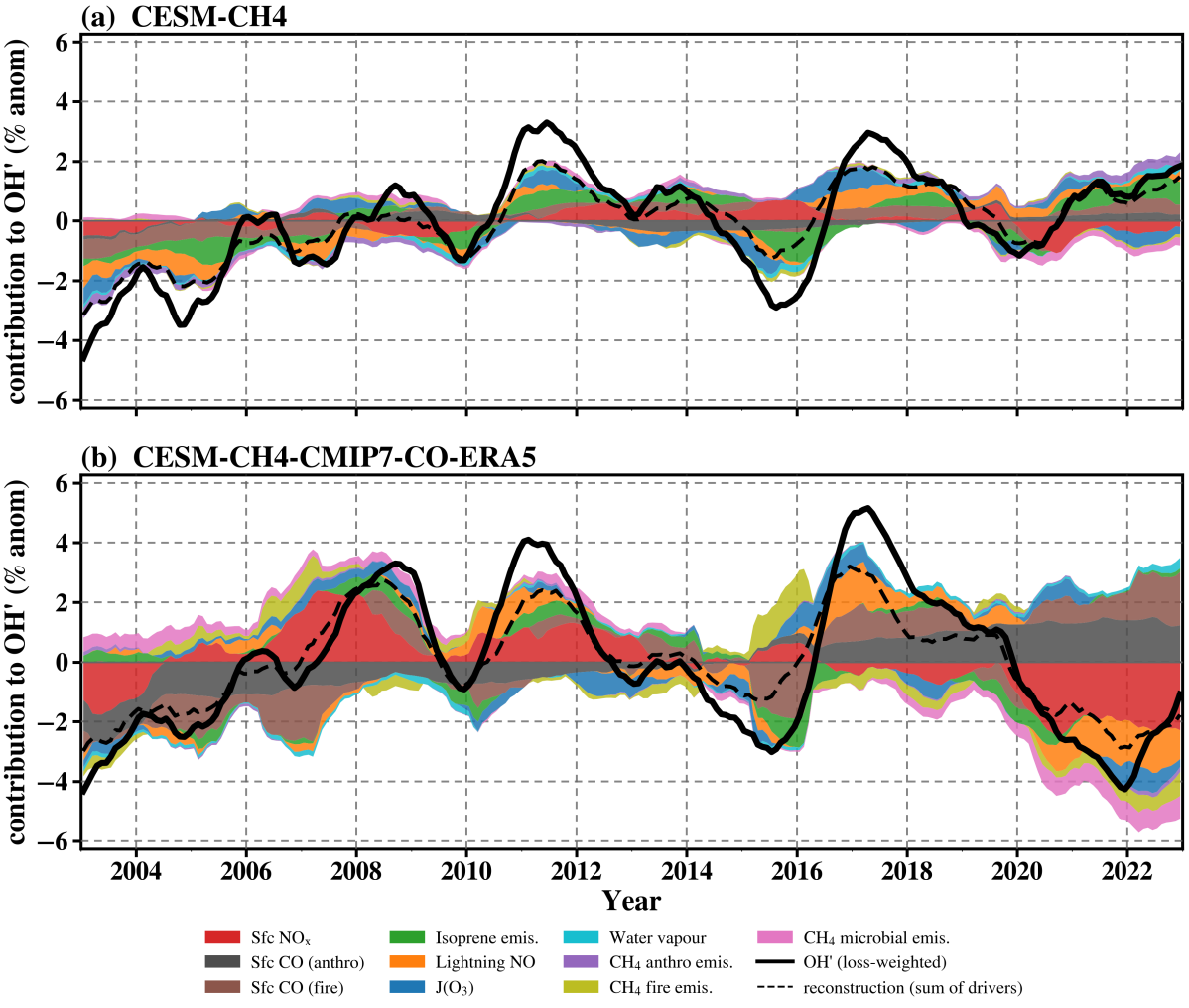

Figure 11. Driver contributions to the global, loss-weighted OH anomaly in the *forcing* basis, for (a) CESM-CH4 and (b) CESM-CH4-CMIP7-CO-ERA5. Bands are the stacked per-driver contributions (% anomaly). The black line is OH′ and the dashed line its reconstruction (the sum of the coloured bands)

https://doi.org/10.5194/egusphere-2026-4883
Preprint. Discussion started: 14 August 2026

The study period opens with both configurations at their most negative OH anomaly (about -3.5 % in 2003), but for opposite budget reasons. In CESM-CH4 the high early-record CO burden, keeps the CO+OH sink large and holds OH down, and the regression assigns this suppression to the CO burden (Figure 12a) and, in the forcing basis, to fire CO (Figure 11a), as FINN emissions are high for this period. In CESM-CH4-CMIP7-CO-ERA5, the same low OH instead comes from weak primary production, with O(^{1}D)+H_2O and the NO_x-recycling source both negative. The two runs therefore track one another in these years while being controlled by different terms, a coincidence of sign rather than of mechanism. The differences in surface NO_x emissions might explain the larger role of NO_x in the simulation driven by CMIP7 emissions (CESM-CH4-CMIP7-CO-ERA5, Figure 2). OH then recovers through 2006–2008 as the CO+OH sink relaxes (-2.8 Tmol yr^{-1} in CESM-CH4 by 2008) and, in the CESM-CH4-CMIP7-CO-ERA5 configuration, as the NO_x-recycling source strengthens. The recovery is stronger and a year earlier in CESM-CH4-CMIP7-CO-ERA5. The record-high OH of 2011 is reached by both runs together (within 0.4 %). The 2010–2011 La Niña draws the CO burden down and reduces the CO+OH sink. The regression shows that the falling CO burden carries the peak in both experiments, with the forcing basis attributing it to reduced fire CO emission. This is a clear case in which ENSO related CO swing controls both configurations, consistent with the ENSO pacing of interannual OH reported previously (Prinn et al., 2001; Anderson et al., 2021). We also found that the biogenic emissions are also lower in 2011 (Figure 2) and it is reflected by a contribution of isoprene to the positive OH anomalies, which could have impacted further the CO impacts seen in the burden based regression.

After a mild relaxation in 2012–2014, OH drops sharply in 2015 (-2.6 and -2.9 %) as the developing 2015–2016 El Niño and the Indonesian fires increase the CO burden and raise the CO+OH sink (Yin et al., 2016). The increase in sink is large enough here to dominate a rising production by biogenic emissions, even in the production-controlled ERA5 run, so the two again move together. The configurations first diverge in 2016 to 2019, when CESM-CH4-CMIP7-CO-ERA5 sits about 1.8 % higher. In the high-ozone and high-lightning, OH production strengthens which the forcing regression attributes the rise to stronger surface and lightning NO_x and the J(O_3) photolysis term during these weak negative anomalies (Murray et al., 2013; Turner et al., 2018), and the burden regression to the rising O_3 and NO_2 burdens. The reduced fire emissions also have a role in the positive OH anomaly. CESM-CH4 increases less, and a year later, its 2017 maximum coming from a CO-sink reduction rather than the production surge. OH stays elevated through 2018–2019, more in the CESM-CH4-CMIP7-CO-ERA5 experiment than in CESM-CH4, where larger biogenic emissions and fire reduces OH.

As quantified in Section 5, the OH-driven contribution to the 2020 growth is moderate in comparison to several studies in the literature (Brasseur and Gaubert, 2025). OH production collapses, with O(^{1}D)+H_2O down by $-2.3/-3.2$ and the NO_x-recycling source decrease by $-1.5/-1.9$ Tmol yr^{-1}. The regression shows a simultaneous decline in the surface NO_x forcing, in line with the COVID-19 emission reductions (Gaubert et al., 2021; Miyazaki et al., 2021) and an extended fire season that started with the Australian fires (Chen et al., 2025), but was also larger than usual during the boreal summer (Ortega et al., 2023), and over the Amazon (Libonati et al., 2021). Here we find a conflicting but interesting role of meteorologically driven anomalies of lightning NOx, with a negative anomaly in ERA5 driven simulation after 2020, as discussed earlier (Fig. 11b). Under CESM-CH4-CMIP7-CO-ERA5 the convective lightning source does not offset the surface-NO_x reduction as it does under CESM-CH4 (MERRA-2), so the NO_x-recycling pathway drops, whereas in CESM-CH4, sources and sinks are

https://doi.org/10.5194/egusphere-2026-4883
Preprint. Discussion started: 14 August 2026

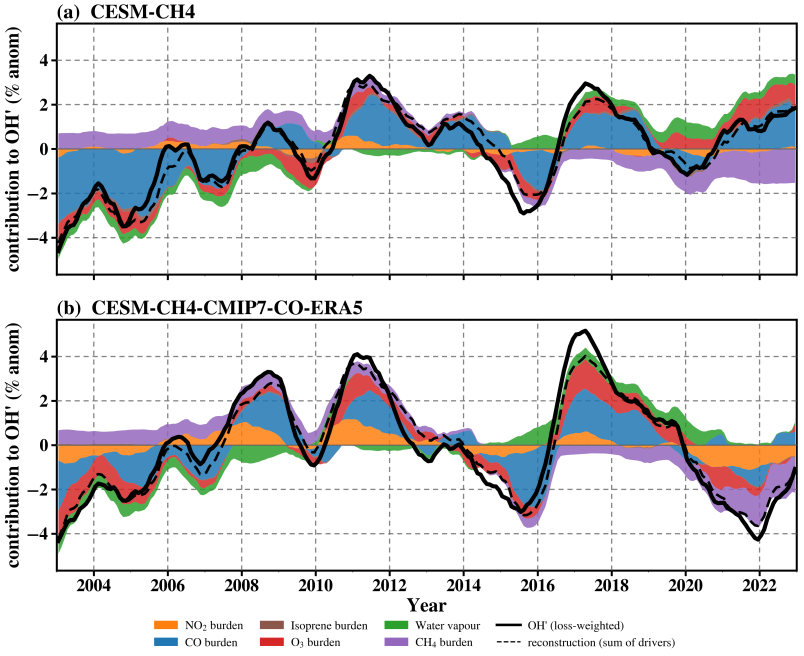

Figure 12. Driver contributions to the global, loss-weighted OH anomaly in the *burden* basis (the CO, NO_2, O_3, isoprene and CH_4 burdens and water vapour), for (a) CESM-CH4 and (b) CESM-CH4-CMIP7-CO-ERA5. Bands are the stacked per-driver contributions (% anomaly); the black line is OH' and the dashed line its reconstruction (the sum of the coloured bands)

510 balanced and there is a low OH interannual variability. Both simulations show elevated biogenic isoprene that consumes OH and suppresses ozone (in the absence of NO_x), in line with a recent study using CrIS isoprene data (Yoon et al., 2025) or the idealized aquaplanet version of CAM-chem (Aqua-chem, Zhu et al., 2026). In the 2020 case, the impact on the burdens corresponds to reduced O_3 and NO_2 burdens (Figure 12b), a process well documented (e.g., Bouarar et al., 2021).

The simulations diverge decisively after 2020, when OH in the CESM-CH4 stays mildly positive while CESM-CH4-CMIP7-
515 CO-ERA5 plunges with continued lower lightning emissions. There are also important differences with reduced surface anthropogenic NO_x in CMIP7 emissions (that are not recovering after 2020) and different biomass-burning emissions emerging in the fire-CO terms, most notably in 2021 (Figure 11). This lower OH in the CESM-CH4-CMIP7-CO-ERA5 simulations drives the higher CH_4 growth rate during these years (Section 7).

Finally, to assess the influence of the El Niño–Southern Oscillation (ENSO) on OH variability, we correlated the loss-
520 weighted OH anomaly with the MEI.v2 index (Wolter and Timlin, 2011). In the sink-controlled CESM-CH4 simulation, OH is significantly anti-correlated with ENSO (annual $r = -0.63$, $p = 0.01$), with lower OH during El Niño conditions and high OH during La Niña. Monthly cross-correlation analysis shows the strongest relationship when ENSO lags OH by approximately 2–4 months. The CO burden behaves consistently, showing a positive correlation with ENSO ($r = +0.40$ with MEI.v2) and a negative correlation with OH (Fig. S10). These results are consistent with methyl chloroform constraints reported by Patra

https://doi.org/10.5194/egusphere-2026-4883
Preprint. Discussion started: 14 August 2026

et al. (2021), who found the CH_4 loss rate to be anti-correlated with the same ENSO index ($r = -0.29$ to -0.38, with lags of 3–8 months), although the simulated response in CESM-CH4 is stronger. In the OH production-controlled CESM-CH4-CMIP7-CO-ERA5 simulation, the correlation weakens substantially ($r = -0.25$), indicating that variability in lightning NO_x (and related O_3-driven) OH production partially offsets the ENSO-driven sink response. An example occurs during 2020-2022, when OH decreases despite persistent La Niña conditions that would otherwise favour higher OH. In this period, the emission and meteorology-driven OH production reduction highlighted by Ciais et al. (2026) and Zhao et al. (2025a) appear to override the ENSO impact on OH sinks. Because of buffering impact with interactive OH, its impact on CH_4 growth rate is at most about one-fifth of the 2020-2022 CH_4 growth rate anomaly in the two best experiments, which is substantially smaller than the $\sim 80\,\%$ contribution inferred from prescribed-OH inversions (CT-CH4-2025). Future work should focus on better quantifying the regional to continental differences in OH driven by ENSO (Shutter et al., 2024).

7 Conclusions

We summarize the findings of this study as follows:

1. While CH_4+OH reaction is estimated to contribute to about 13 % of the OH loss, here calculated for the year 2013, the slow burden evolution of CH_4 suggests that it contributes relatively little to interannual OH variability. A simulation in which the CH_4 emissions were kept at the 2003 levels throughout our 20-year period, the average OH was only reduced by 0.4 % over that period. We compared one emission- and one concentration-driven simulation, which had a similar CH_4 burden, but with a different spatial and temporal distribution. They showed no differences in annual and global CH_4 chemical lifetime with respect to tropospheric OH.

2. In contrast, using established emission inventories (CAMS/FINN2.5 vs. CEDS-CMIP7) with different spatial distributions, chemical speciation, and temporal variation led to a net 10 % difference in OH between simulations on average during the 2003-2022 period. This resulted in an 8 % shorter CH_4 lifetime in the CMIP7 configuration, which caused a strong bias in simulated CH_4.

3. This study presents the first comparison of nudging the CAM-chem model to the hourly ERA5 reanalysis dataset. The switch from the MERRA-2 3-hourly dataset has a comparable impact in magnitude on OH levels to the complete anthropogenic and fire emission inventory swap. The CH_4 lifetime is increased by 9.3 % when using ERA5 due to stronger biogenic emission. Despite the pair of simulations using the same set of emissions, the CH_4 chemical loss is reduced by 20 $TgCH_4$ yr^{-1} and the atmospheric growth rate is increased from around 10 $TgCH_4$ yr^{-1} to 23 $TgCH_4$ yr^{-1}. In this case, the simulation nudged to ERA5 is much closer to the observed growth rate. On average, the impact of meteorology on OH results from offsets in vegetation emissions, as estimated by the MEGAN model, which are strongly sensitive to temperature and radiation. These biogenic emissions have a large impact through a cascade of reactions involving isoprene and other organic compounds that effectively reduce OH and ultimately increase CO. There is a clear recycling of OH through increased OVOCs and H_2O_2 sources of OH.

https://doi.org/10.5194/egusphere-2026-4883
Preprint. Discussion started: 14 August 2026

4. We find that the two reanalysis datasets produce a strong difference in lightning NO_x emissions over the 2020–2022 period, resulting in large uncertainties in CH_4 lifetime anomalies. In contrast, the differences in biogenic emissions presented here are nearly time invariant and primarily reduce OH in the ERA5-driven simulations. Previous studies have shown that meteorological nudging affects mean OH concentrations rather than OH interannual variability or decadal trends (Gaubert et al., 2017; He et al., 2021). Our results suggest that reanalysis-dependent differences in lightning NO_x emissions can nevertheless introduce substantial uncertainty in OH and CH_4 lifetime anomalies during specific periods.

5. Because the two best configurations share the same CH_4 emissions, their OH difference imprints directly on the year-to-year growth rate, and the OH-driven contribution to the 2020-2022 surge spans from near zero (MERRA-2) to about one fifth of the growth (ERA5). While the ERA5 run reproduces the overall elevated CH_4 growth better, the year-by-year comparison with NOAA GML measurements suggests that its OH reduction may be somewhat too strong in the peak years of 2020-2022, or that the posterior CH_4 emissions used here are overestimated.

6. The interannual OH variability is governed by different contributions: the CESM-CH4 run shows larger sensitivity to the CO burden controling the OH sink, while the ERA5 run is more sensitive to the production of OH from the $O(^1D)$+H_2O and NO_x sources. The two simulations therefore agree when an ENSO-paced swing in emissions of fire CO, biogenic NMVOCs and lightning NO_x dominates (2011, 2015) and diverge when meteorology varies (2016-2017 and, most strongly, 2020-2022). A loss-weighted global linear regression confirms that this OH interannual variability is set by NO_x, CO, and ozone photochemistry rather than by the CH_4 fluxes.

7. For 2020, the two simulations attribute an OH-driven CH_4 forcing of $+1.4$ ppb yr^{-1} (≈ 4 Tg a^{-1}; about 12 % of the emission-plus-OH forcing $\Delta E - m\,\Delta k$) in CESM-CH4 and $+4.8$ ppb yr^{-1} (≈ 13 Tg a^{-1}; about 31 %) in CESM-CH4-CMIP7-CO-ERA5. The CESM-CH4 estimate is close to the 5 Tg a^{-1} (14 %) reported by Qu et al. (2022), but lower than other studies that quantify an impact of OH closer to 50 % (Stevenson et al., 2022; Peng et al., 2022; Chen et al., 2025).

8. During our 20-year study period, tropospheric OH reached its largest positive anomalies (more than 3 %) in 2011 and 2017, associated with lower biogenic emissions, higher lightning NO_x, and lower fire CO emissions. Because the OH forcing on the growth rate depends on the year-to-year change in OH rather than its absolute level, the largest OH-driven reductions in the CH_4 growth rate occur when OH rose most steeply, about 4 ppb yr^{-1} during the 2011 increase and up to 7 ppb yr^{-1} in 2016, as OH climbed toward the 2017 maximum. Both exceeded the 2020 OH contribution. Conversely, 2015 stands out as a low-OH year, during the 2015—2016 El Niño, in which weaker oxidation raised the CH_4 growth rate.

We find that OH is well buffered against chemistry perturbations, as increased chemical complexity raises the OH recycling probability. Consequently, studies relying on simplified and prescribed OH representations may neglect these complex chemical feedbacks and overestimate the role of OH changes in driving the CH_4 growth rate. This relatively weaker role of OH implies that the atmospheric CH_4 growth rate is mainly controlled by direct CH_4 emissions, which should be the focus of mitigation for climate targets (Shindell et al., 2024).

https://doi.org/10.5194/egusphere-2026-4883
Preprint. Discussion started: 14 August 2026

This study highlights that further work is needed to reduce OH uncertainties, which will be critical to improve estimates of the CH_4 budget, but also for the Earth's tropospheric chemistry system as a whole. This can be achieved by an improved understanding of tropospheric chemistry and OH reactivity (Travis et al., 2020; Fuchs et al., 2025; Price et al., 2025; Tan et al., 2026), a better characterization (Strode et al., 2026; Nicely et al., 2018) and uncertainty quantification (Murray et al., 2021; Wild and Ryan, 2026) of the OH drivers across models, as well as innovative use of multiple satellite observations (Duncan et al., 2024; Anderson et al., 2022; Souri et al., 2024; Shutter et al., 2024). Also, our improved modelling framework is also well suited to assess the direct and indirect effects of molecular hydrogen (H_2) on OH, and hence on the CH_4 budget (Bryant and Stevenson, 2024; Yang et al., 2025; Chua et al., 2025), an effect of growing importance as the hydrogen economy expands.

Code and data availability. The posterior CO emission flux resulting from inverse modelling of MOPITT CO data are available for download (Gaubert, 2024). The NOAA CarbonTracker-CH4 2025 posterior CH_4 fluxes are available for download (Oh et al., 2025). The TROPOMI CO data can be found at https://doi.org/10.5270/s5p-bj3nry0. The MEIv2 can be downloaded at www.esrl.noaa.gov/psd/enso/mei/. GOSAT Proxy v9.0 X data are available from the Centre for Environmental Data Analysis data repository at https://catalogue.ceda.ac.uk/uuid/18ef8247f52a4cb6a14013f8235cc1eb/. Blended TROPOMI+GOSAT CH_4 data are available for download at https://registry.opendata.aws/blended-tropomi-gosat-methane. The CAMS anthropogenic emissions are available from the ECCAD emissions database, at eccad.sedoo.fr.

Appendix A: Chemistry updates

The methyl peroxy radical (CH_3O_2) reaction with OH has been proposed to be important by Archibald et al. (2009) and has been implemented in global models (e.g., Bates et al., 2021). Assaf et al. (2017) performed laboratory measurements and identified that previous yield of methanol of up to 30 % from (Müller et al., 2016) and the reaction rate (Bossolasco et al., 2014) were likely overestimated. Here, we calculate the average of the reaction rate between Yan et al. (2016) and Assaf et al. (2017) and we obtain k = 1.2 10^{-10} cm^3 $molecule^{-1}$ s^{-1}. Assuming the alkoxy (CH_3O) intermediate reacts rapidly with O_2 to produce formaldehyde and HO_2, and (for simplicity) redistributing the CH_3OOOH adduct product between CH_3OH and CH_2O, thus we obtain:

$$CH_3O_2 + OH + 0.89 * O_2 \rightarrow 0.11 * CH_3OH + 0.11 * O_2 + 1.78 * HO_2 + 0.89 * CH_2O; k = 1.210^{-10} cm^3 molecule^{-1} s^{-1} \quad \text{(AR1)}$$

Our low yield of 11% of CH_3OH is closer to the GEOS-chem implementation of 13 % from Bates et al. (2021).

Author contributions. Conceptualization: BG and MAM; Data curation: BG and MAM; Formal analysis: BG and MAM; Funding acquisition: BG and AFA; Investigation: BG and MAM; Methodology: BG and MAM; Project administration: BG and AFA; Software: BG, MAM, RF; Supervision: BG and AFA; Validation: BG and MAM; Visualization: BG and MAM; Writing (original draft preparation): BG and MAM; Writing (review and editing): BG, MAM, YX, AFA, YO, IO, RF, JO, GP, XL, GB

https://doi.org/10.5194/egusphere-2026-4883
Preprint. Discussion started: 14 August 2026

Competing interests. The authors declare no competing interests.

Acknowledgements. This study was supported by NOAA Climate Program Office's Atmospheric Chemistry, Carbon Cycle, and Climate program, grant numbers NA23OAR4310285 and NA24OARX431G0009. This material is based upon work supported by the NSF National Center for Atmospheric Research, which is a major facility sponsored by the National Science Foundation under Cooperative Agreement No. 1755088 and No. 1852977. Any opinions, findings and conclusions or recommendations expressed in this material do not necessarily reflect the views of the National Science Foundation. We would like to acknowledge high-performance computing support from the Derecho system (Computational and Information Systems Laboratory, 2023) provided by the NSF National Center for Atmospheric Research (NSF NCAR), sponsored by the National Science Foundation. The NDACC effort at NSF NCAR is supported under contract by NASA. We thank the HIPPO, ATom, KORUS-AQ, and ACCLIP teams for providing aircraft data. We thank Kathryn McKain for helpful comments on the manuscript.

https://doi.org/10.5194/egusphere-2026-4883
Preprint. Discussion started: 14 August 2026

References

Akimoto, H. and Tanimoto, H.: Rethinking of the adverse effects of NOx-control on the reduction of methane and tropospheric ozone – Challenges toward a denitrified society, Atmospheric Environment, 277, 119 033, https://doi.org/10.1016/j.atmosenv.2022.119033, 2022.

Allen, R. J., Horowitz, L. W., Naik, V., Oshima, N., O'Connor, F. M., Turnock, S., Shim, S., Le Sager, P., van Noije, T., Tsigaridis, K., Bauer, S. E., Sentman, L. T., John, J. G., Broderick, C., Deushi, M., Folberth, G. A., Fujimori, S., and Collins, W. J.: Significant climate benefits from near-term climate forcer mitigation in spite of aerosol reductions, Environmental Research Letters, https://doi.org/10.1088/1748-9326/abe06b, 2021.

Anderson, D. C., Duncan, B. N., Fiore, A. M., Baublitz, C. B., Follette-Cook, M. B., Nicely, J. M., and Wolfe, G. M.: Spatial and temporal variability in the hydroxyl (OH) radical: understanding the role of large-scale climate features and their influence on OH through its dynamical and photochemical drivers, Atmospheric Chemistry and Physics, 21, 6481–6508, https://doi.org/10.5194/acp-21-6481-2021, 2021.

Anderson, D. C., Follette-Cook, M. B., Strode, S. A., Nicely, J. M., Liu, J., Ivatt, P. D., and Duncan, B. N.: A machine learning methodology for the generation of a parameterization of the hydroxyl radical, Geoscientific Model Development, 15, 6341–6358, https://doi.org/10.5194/gmd-15-6341-2022, 2022.

Archibald, A. T., Petit, A. S., Percival, C. J., Harvey, J. N., and Shallcross, D. E.: On the importance of the reaction between OH and RO₂ radicals, Atmospheric Science Letters, 10, 102–108, https://doi.org/10.1002/asl.216, 2009.

Assaf, E., Sheps, L., Whalley, L., Heard, D., Tomas, A., Schoemaecker, C., and Fittschen, C.: The Reaction between CH_3O_2 and OH Radicals: Product Yields and Atmospheric Implications, Environmental Science & Technology, 51, 2170–2177, https://doi.org/10.1021/acs.est.6b06265, 2017.

Balasus, N., Jacob, D. J., Lorente, A., Maasakkers, J. D., Parker, R. J., Boesch, H., Chen, Z., Kelp, M. M., Nesser, H., and Varon, D. J.: A blended TROPOMI+GOSAT satellite data product for atmospheric methane using machine learning to correct retrieval biases, Atmospheric Measurement Techniques, 16, 3787–3807, https://doi.org/10.5194/amt-16-3787-2023, 2023.

Balasus, N., Jacob, D. J., Bloom, A. A., East, J. D., Estrada, L. A., Hancock, S. E., He, M., Mooring, T. A., Turner, A. J., and Worden, J. R.: 2019–2024 trends in African livestock and wetland emissions as contributors to the global methane rise, Atmospheric Chemistry and Physics, 26, 4601–4617, https://doi.org/10.5194/acp-26-4601-2026, 2026.

Basu, S., Lan, X., Dlugokencky, E., Michel, S., Schwietzke, S., Miller, J. B., Bruhwiler, L., Oh, Y., Tans, P. P., Apadula, F., Gatti, L. V., Jordan, A., Necki, J., Sasakawa, M., Morimoto, S., Di Iorio, T., Lee, H., Arduini, J., and Manca, G.: Estimating emissions of methane consistent with atmospheric measurements of methane and δ^{13}C of methane, Atmospheric Chemistry and Physics, 22, 15 351–15 377, https://doi.org/10.5194/acp-22-15351-2022, 2022.

Bates, K. H., Jacob, D. J., Wang, S., Hornbrook, R. S., Apel, E. C., Kim, M. J., Millet, D. B., Wells, K. C., Chen, X., Brewer, J. F., Ray, E. A., Commane, R., Diskin, G. S., and Wofsy, S. C.: The Global Budget of Atmospheric Methanol: New Constraints on Secondary, Oceanic, and Terrestrial Sources, Journal of Geophysical Research: Atmospheres, 126, https://doi.org/10.1029/2020jd033439, 2021.

Belikov, D. A., Patra, P. K., and Saitoh, N.: Hydroxyl Interannual Variability Impacts Estimation of Regional Methane Emissions, Journal of Geophysical Research: Atmospheres, 131, https://doi.org/10.1029/2025jd044457, 2026.

Borsdorff, T., Aan de Brugh, J., Hu, H., Aben, I., Hasekamp, O., and Landgraf, J.: Measuring Carbon Monoxide With TROPOMI: First Results and a Comparison With ECMWF-IFS Analysis Data, Geophysical Research Letters, 45, 2826–2832, https://doi.org/10.1002/2018gl077045, 2018.

https://doi.org/10.5194/egusphere-2026-4883
Preprint. Discussion started: 14 August 2026

Bossolasco, A., Faragó, E. P., Schoemaecker, C., and Fittschen, C.: Rate constant of the reaction between CH3O2 and OH radicals, Chemical Physics Letters, 593, 7–13, https://doi.org/10.1016/j.cplett.2013.12.052, 2014.

Bossolasco, A., Fernandez, R. P., Li, Q., Mahajan, A. S., Villamayor, J., Barrera, J. A., Heard, D. E., Cuevas, C. A., Caram, C., Szopa, S., and Saiz-Lopez, A.: Key role of short-lived halogens on global atmospheric oxidation during historical periods, Environmental Science: Atmospheres, https://doi.org/10.1039/d4ea00141a, 2025.

Bouarar, I., Gaubert, B., Brasseur, G. P., Steinbrecht, W., Doumbia, T., Tilmes, S., Liu, Y., Stavrakou, T., Deroubaix, A., Darras, S., Granier, C., Lacey, F., Müller, J.-F., Shi, X., Elguindi, N., and Wang, T.: Ozone Anomalies in the Free Troposphere During the COVID-19 Pandemic, Geophysical Research Letters, 48, https://doi.org/10.1029/2021gl094204, 2021.

Bouarar, I., Granier, C., Denier van der Gon, H., Doumbia, T., Guevara, M., Jalkanen, J.-P., Kuenen, J., Majamäki, E., Zilbermann, N., and Brasseur, G.: Refining the CAMS Global Anthropogenic Emissions Inventory with Regional Datasets: Advances in the Mosaic Approach and Remaining Uncertainties, https://doi.org/10.5194/egusphere-egu26-9863, 2026.

Brasseur, G. P. and Gaubert, B.: The atmospheric oxidizing capacity and the methane budget, National Science Review, 12, https://doi.org/10.1093/nsr/nwaf347, 2025.

Bryant, H. and Stevenson, D.: The influence of hydrogen on carbon monoxide in the troposphere, Weather, 79, 190–195, https://doi.org/10.1002/wea.4567, 2024.

Chandra, N., Patra, P. K., Fujita, R., Höglund-Isaksson, L., Umezawa, T., Goto, D., Morimoto, S., Vaughn, B. H., and Röckmann, T.: Methane emissions decreased in fossil fuel exploitation and sustainably increased in microbial source sectors during 1990–2020, Communications Earth & Environment, 5, https://doi.org/10.1038/s43247-024-01286-x, 2024.

Chen, W., Zhang, Y., and Liang, R.: Converging evidence for reduced global atmospheric oxidation in 2020, National Science Review, 12, https://doi.org/10.1093/nsr/nwaf232, 2025.

Chua, G., Naik, V., and Horowitz, L. W.: Exploring the drivers of tropospheric hydroxyl radical trends in the Geophysical Fluid Dynamics Laboratory AM4.1 atmospheric chemistry–climate model, Atmospheric Chemistry and Physics, 23, 4955–4975, https://doi.org/10.5194/acp-23-4955-2023, 2023.

Chua, G., Naik, V., Paulot, F., Feng, J., and Horowitz, L. W.: Impact of Future Methane Emission Trajectories on Atmospheric Composition and Climate in a Future Hydrogen Economy, Earth's Future, 13, https://doi.org/10.1029/2025ef006254, 2025.

Ciais, P., Zhu, Y., Cai, Y., Lan, X., Michel, S. E., Zheng, B., Zhao, Y., Hauglustaine, D. A., Lin, X., Zhang, Y., Sun, S., Tian, X., Zhao, M., Wang, Y., Chang, J., Dou, X., Liu, Z., Andrew, R., Quinn, C. A., Poulter, B., Ouyang, Z., Yuan, W., Yuan, K., Zhu, Q., Li, F., Pan, N., Tian, H., Yu, X., Rocher-Ros, G., Johnson, M. S., Li, M., Li, M., Feng, D., Raymond, P., Yang, X., Canadell, J. G., Jackson, R. B., Yu, X., Li, Y., Saunois, M., Bousquet, P., and Peng, S.: Why methane surged in the atmosphere during the early 2020s, Science, 391, https://doi.org/10.1126/science.adx8262, 2026.

Computational and Information Systems Laboratory: Derecho: HPE Cray EX Cluster, https://doi.org/10.5065/QX9A-PG09, 2023.

Crawford, J. H., Ahn, J.-Y., Al-Saadi, J., Chang, L., Emmons, L. K., Kim, J., Lee, G., Park, J.-H., Park, R. J., Woo, J. H., Song, C.-K., Hong, J.-H., Hong, Y.-D., Lefer, B. L., Lee, M., Lee, T., Kim, S., Min, K.-E., Yum, S. S., Shin, H. J., Kim, Y.-W., Choi, J.-S., Park, J.-S., Szykman, J. J., Long, R. W., Jordan, C. E., Simpson, I. J., Fried, A., Dibb, J. E., Cho, S., and Kim, Y. P.: The Korea-United States Air Quality (KORUS-AQ) field study, Elementa: Science of the Anthropocene, 9, https://doi.org/10.1525/elementa.2020.00163, 2021.

Crutzen, P. J. and Zimmermann, P. H.: The changing photochemistry of the troposphere, Tellus B: Chemical and Physical Meteorology, 43, 136, https://doi.org/10.3402/tellusb.v43i4.15403, 1991.

https://doi.org/10.5194/egusphere-2026-4883
Preprint. Discussion started: 14 August 2026

Danabasoglu, G., Lamarque, J.-F., Bacmeister, J., Bailey, D. A., DuVivier, A. K., Edwards, J., Emmons, L. K., Fasullo, J., Garcia, R., Gettelman, A., Hannay, C., Holland, M. M., Large, W. G., Lauritzen, P. H., Lawrence, D. M., Lenaerts, J. T. M., Lindsay, K., Lipscomb, W. H., Mills, M. J., Neale, R., Oleson, K. W., Otto-Bliesner, B., Phillips, A. S., Sacks, W., Tilmes, S., Kampenhout, L., Vertenstein, M., Bertini, A., Dennis, J., Deser, C., Fischer, C., Fox-Kemper, B., Kay, J. E., Kinnison, D., Kushner, P. J., Larson, V. E., Long, M. C., Mickelson, S., Moore, J. K., Nienhouse, E., Polvani, L., Rasch, P. J., and Strand, W. G.: The Community Earth System Model Version 2 (CESM2), Journal of Advances in Modeling Earth Systems, 12, https://doi.org/10.1029/2019ms001916, 2020.

Davis, N. A., Callaghan, P., Simpson, I. R., and Tilmes, S.: Specified dynamics scheme impacts on wave-mean flow dynamics convection and tracer transport in CESM2 (WACCM6), Atmospheric Chemistry and Physics, 22, 197–214, https://doi.org/10.5194/acp-22-197-2022, 2022.

De Mazière, M., Thompson, A. M., Kurylo, M. J., Wild, J. D., Bernhard, G., Blumenstock, T., Braathen, G. O., Hannigan, J. W., Lambert, J.-C., Leblanc, T., McGee, T. J., Nedoluha, G., Petropavlovskikh, I., Seckmeyer, G., Simon, P. C., Steinbrecht, W., and Strahan, S. E.: The Network for the Detection of Atmospheric Composition Change (NDACC): history, status and perspectives, Atmospheric Chemistry and Physics, 18, 4935–4964, https://doi.org/10.5194/acp-18-4935-2018, 2018.

Dean, J. F., Middelburg, J. J., Röckmann, T., Aerts, R., Blauw, L. G., Egger, M., Jetten, M. S. M., de Jong, A. E. E., Meisel, O. H., Rasigraf, O., Slomp, C. P., in't Zandt, M. H., and Dolman, A. J.: Methane Feedbacks to the Global Climate System in a Warmer World, Reviews of Geophysics, 56, 207–250, https://doi.org/10.1002/2017rg000559, 2018.

Deeter, M. N., Francis, G., Gille, J., Mao, D., Martínez-Alonso, S., Worden, H., Ziskin, D., Drummond, J., Commane, R., Diskin, G., and McKain, K.: The MOPITT Version 9 CO product: sampling enhancements and validation, Atmospheric Measurement Techniques, 15, 2325–2344, https://doi.org/10.5194/amt-15-2325-2022, 2022.

Dlugokencky, E. J., Bruhwiler, L., White, J. W. C., Emmons, L. K., Novelli, P. C., Montzka, S. A., Masarie, K. A., Lang, P. M., Crotwell, A. M., Miller, J. B., and Gatti, L. V.: Observational constraints on recent increases in the atmospheric CH4 burden, Geophysical Research Letters, 36, https://doi.org/10.1029/2009gl039780, 2009.

Drummond, J. R., Zou, J., Nichitiu, F., Kar, J., Deschambaut, R., and Hackett, J.: A review of 9-year performance and operation of the MOPITT instrument, Advances in Space Research, 45, 760–774, https://doi.org/10.1016/j.asr.2009.11.019, 2010.

Duncan, B. N., Anderson, D. C., Fiore, A. M., Joiner, J., Krotkov, N. A., Li, C., Millet, D. B., Nicely, J. M., Oman, L. D., St. Clair, J. M., Shutter, J. D., Souri, A. H., Strode, S. A., Weir, B., Wolfe, G. M., Worden, H. M., and Zhu, Q.: Opinion: Beyond global means – novel space-based approaches to indirectly constrain the concentrations of and trends and variations in the tropospheric hydroxyl radical (OH), Atmospheric Chemistry and Physics, 24, 13 001–13 023, https://doi.org/10.5194/acp-24-13001-2024, 2024.

Emmons, L. K., Schwantes, R. H., Orlando, J. J., Tyndall, G., Kinnison, D., Lamarque, J.-F., Marsh, D., Mills, M. J., Tilmes, S., Bardeen, C., Buchholz, R. R., Conley, A., Gettelman, A., Garcia, R., Simpson, I., Blake, D. R., Meinardi, S., and Pétron, G.: The Chemistry Mechanism in the Community Earth System Model Version 2 (CESM2), Journal of Advances in Modeling Earth Systems, 12, https://doi.org/10.1029/2019ms001882, 2020.

Feng, L., Smith, S. J., Braun, C., Crippa, M., Gidden, M. J., Hoesly, R., Klimont, Z., van Marle, M., van den Berg, M., and van der Werf, G. R.: The generation of gridded emissions data for CMIP6, Geoscientific Model Development, 13, 461–482, https://doi.org/10.5194/gmd-13-461-2020, 2020.

Feng, L., Palmer, P. I., Wang, H., Parker, R., Boesch, H., Biraud, S. C., Chmura, , Gloor, E., Haszpra, L., Kozlova, E., Nisbet, E. G., Noe, S. M., Röckmann, T., Ferreira de Souza, R. A., and Steinbacher, M.: Atmospheric methane growth rates, 2018-2024, driven mainly by emission changes but atmospheric photochemistry is important, egusphere, https://doi.org/10.5194/egusphere-2026-2662, 2026.

https://doi.org/10.5194/egusphere-2026-4883
Preprint. Discussion started: 14 August 2026

Fernandez, R. P., Cuevas, C. A., Villamayor, J., Feinberg, A., Kinnison, D. E., Vitt, F., Bossolasco, A., Barrera, J. A., Reynoso, A., Tomazzeli, O. G., Li, Q., and Saiz-Lopez, A.: Short-Lived Halogen Sources and Chemistry in the Community Earth System Model v2 (CESM2-SLH), EGUsphere [preprint], https://doi.org/10.5194/egusphere-2025-3250, 2025.

Fiore, A. M., Jacob, D. J., Field, B. D., Streets, D. G., Fernandes, S. D., and Jang, C.: Linking ozone pollution and climate change: The case for controlling methane, Geophysical Research Letters, 29, https://doi.org/10.1029/2002gl015601, 2002.

Fiore, A. M., Horowitz, L. W., Dlugokencky, E. J., and West, J. J.: Impact of meteorology and emissions on methane trends, 1990–2004, Geophysical Research Letters, 33, https://doi.org/10.1029/2006gl026199, 2006.

Fiore, A. M., Hancock, S. E., Lamarque, J.-F., Correa, G. P., Chang, K.-L., Ru, M., Cooper, O., Gaudel, A., Polvani, L. M., Sauvage, B., and Ziemke, J. R.: Understanding recent tropospheric ozone trends in the context of large internal variability: a new perspective from chemistry-climate model ensembles, Environmental Research: Climate, 1, 025 008, https://doi.org/10.1088/2752-5295/ac9cc2, 2022.

Folberth, G. A., Staniaszek, Z., Archibald, A. T., Gedney, N., Griffiths, P. T., Jones, C. D., O'Connor, F. M., Parker, R. J., Sellar, A. A., and Wiltshire, A.: Description and Evaluation of an Emission-Driven and Fully Coupled Methane Cycle in UKESM1, Journal of Advances in Modeling Earth Systems, 14, https://doi.org/10.1029/2021ms002982, 2022.

Folberth, G. A., Jones, C. D., O'Connor, F. M., Gedney, N., Griffiths, P. T., and Wiltshire, A. J.: Drivers of persistent changes in the global methane cycle under aggressive mitigation action, npj Climate and Atmospheric Science, 8, https://doi.org/10.1038/s41612-024-00867-z, 2025.

Froidevaux, L., Kinnison, D. E., Gaubert, B., Schwartz, M. J., Livesey, N. J., Read, W. G., Bardeen, C. G., Ziemke, J. R., and Fuller, R. A.: Tropical upper-tropospheric trends in ozone and carbon monoxide (2005–2020): observational and model results, Atmospheric Chemistry and Physics, 25, 597–624, https://doi.org/10.5194/acp-25-597-2025, 2025.

Fuchs, H., Stainsby, A., Berg, F., Dubus, R., Färber, M., Hofzumahaus, A., Holland, F., Bates, K. H., Brown, S. S., Coggon, M. M., Diskin, G. S., Gkatzelis, G. I., Jernigan, C. M., Peischl, J., Robinson, M. A., Rollins, A. W., Schafer, N. B., Schwantes, R. H., Stockwell, C. E., Veres, P. R., Warneke, C., Waxman, E. M., Xu, L., Zuraski, K., Wahner, A., and Novelli, A.: Advances in an OH reactivity instrument for airborne field measurements, Atmospheric Measurement Techniques, 18, 881–895, https://doi.org/10.5194/amt-18-881-2025, 2025.

Gaubert, B.: Posterior CO emissions, https://doi.org/10.5281/ZENODO.13889018, 2024.

Gaubert, B., Arellano, A. F., Barré, J., Worden, H. M., Emmons, L. K., Tilmes, S., Buchholz, R. R., Vitt, F., Raeder, K., Collins, N., Anderson, J. L., Wiedinmyer, C., Alonso, S. M., Edwards, D. P., Andreae, M. O., Hannigan, J. W., Petri, C., Strong, K., and Jones, N.: Toward a chemical reanalysis in a coupled chemistry-climate model: An evaluation of MOPITT CO assimilation and its impact on tropospheric composition, Journal of Geophysical Research: Atmospheres, 121, 7310–7343, https://doi.org/10.1002/2016jd024863, 2016.

Gaubert, B., Worden, H. M., Arellano, A. F. J., Emmons, L. K., Tilmes, S., Barré, J., Alonso, S. M., Vitt, F., Anderson, J. L., Alkemade, F., Houweling, S., and Edwards, D. P.: Chemical Feedback From Decreasing Carbon Monoxide Emissions, Geophysical Research Letters, 44, 9985–9995, https://doi.org/10.1002/2017gl074987, 2017.

Gaubert, B., Stephens, B. B., Basu, S., Chevallier, F., Deng, F., Kort, E. A., Patra, P. K., Peters, W., Rödenbeck, C., Saeki, T., Schimel, D., der Laan-Luijkx, I. V., Wofsy, S., and Yin, Y.: Global atmospheric CO_2 inverse models converging on neutral tropical land exchange but disagreeing on fossil fuel and atmospheric growth rate, Biogeosciences, 16, 117–134, https://doi.org/10.5194/bg-16-117-2019, 2019.

Gaubert, B., Emmons, L. K., Raeder, K., Tilmes, S., Miyazaki, K., Jr., A. F. A., Elguindi, N., Granier, C., Tang, W., Barré, J., Worden, H. M., Buchholz, R. R., Edwards, D. P., Franke, P., Anderson, J. L., Saunois, M., Schroeder, J., Woo, J.-H., Simpson, I. J., Blake, D. R., Meinardi, S., Wennberg, P. O., Crounse, J., Teng, A., Kim, M., Dickerson, R. R., He, H., Ren, X., Pusede, S. E., and Diskin, G. S.: Correcting model

https://doi.org/10.5194/egusphere-2026-4883
Preprint. Discussion started: 14 August 2026

biases of CO in East Asia: impact on oxidant distributions during KORUS-AQ, Atmospheric Chemistry and Physics, 20, 14 617–14 647, https://doi.org/10.5194/acp-20-14617-2020, 2020.

Gaubert, B., Bouarar, I., Doumbia, T., Liu, Y., Stavrakou, T., Deroubaix, A., Darras, S., Elguindi, N., Granier, C., Lacey, F., Müller, J.-F., Shi, X., Tilmes, S., Wang, T., and Brasseur, G. P.: Global Changes in Secondary Atmospheric Pollutants During the 2020 COVID-19 Pandemic, Journal of Geophysical Research: Atmospheres, 126, https://doi.org/10.1029/2020jd034213, 2021.

Gaubert, B., Anderson, J. L., Trudeau, M., Smith, N., McKain, K., Pétron, G., Raeder, K., Arellano, A. F., Granier, C., Emmons, L. K., Ortega, I., Hannigan, J. W., Tang, W., Worden, H. M., Ziskin, D., and Edwards, D. P.: Nonlinear and Non-Gaussian Ensemble Assimilation of MOPITT CO, Journal of Geophysical Research: Atmospheres, 129, https://doi.org/10.1029/2023jd040647, 2024.

Gelaro, R., McCarty, W., Suárez, M. J., Todling, R., Molod, A., Takacs, L., Randles, C. A., Darmenov, A., Bosilovich, M. G., Reichle, R., Wargan, K., Coy, L., Cullather, R., Draper, C., Akella, S., Buchard, V., Conaty, A., da Silva, A. M., Gu, W., Kim, G.-K., Koster, R., Lucchesi, R., Merkova, D., Nielsen, J. E., Partyka, G., Pawson, S., Putman, W., Rienecker, M., Schubert, S. D., Sienkiewicz, M., and Zhao, B.: The Modern-Era Retrospective Analysis for Research and Applications Version 2 (MERRA-2), Journal of Climate, 30, 5419–5454, https://doi.org/10.1175/jcli-d-16-0758.1, 2017.

Gettelman, A., Mills, M. J., Kinnison, D. E., Garcia, R. R., Smith, A. K., Marsh, D. R., Tilmes, S., Vitt, F., Bardeen, C. G., McInerny, J., Liu, H.-L., Solomon, S. C., Polvani, L. M., Emmons, L. K., Lamarque, J.-F., Richter, J. H., Glanville, A. S., Bacmeister, J. T., Phillips, A. S., Neale, R. B., Simpson, I. R., DuVivier, A. K., Hodzic, A., and Randel, W. J.: The Whole Atmosphere Community Climate Model Version 6 (WACCM6), Journal of Geophysical Research: Atmospheres, 124, 12 380–12 403, https://doi.org/10.1029/2019jd030943, 2019.

Granier, C., Li, C. W. Y., Dellaert, S., Denier van der Gon, H., Doumbia, T., Guevara, M., Jalkanen, J.-P., Kuenen, J., Liousse, C., Majamaki, E., Merly, H., Schoenmakers, E., and Zilbermann, N.: Trends in emissions of atmospheric constituents at the global scale: evaluation and improvements using regional inventories, https://doi.org/10.5194/egusphere-egu25-7386, 2025.

Griffiths, P. T., Murray, L. T., Zeng, G., Shin, Y. M., Abraham, N. L., Archibald, A. T., Deushi, M., Emmons, L. K., Galbally, I. E., Hassler, B., Horowitz, L. W., Keeble, J., Liu, J., Moeini, O., Naik, V., O'Connor, F. M., Oshima, N., Tarasick, D., Tilmes, S., Turnock, S. T., Wild, O., Young, P. J., and Zanis, P.: Tropospheric ozone in CMIP6 simulations, Atmospheric Chemistry and Physics, 21, 4187–4218, https://doi.org/10.5194/acp-21-4187-2021, 2021.

Guenther, A. B., Jiang, X., Heald, C. L., Sakulyanontvittaya, T., Duhl, T., Emmons, L. K., and Wang, X.: The Model of Emissions of Gases and Aerosols from Nature version 2.1 (MEGAN2.1): an extended and updated framework for modeling biogenic emissions, Geoscientific Model Development, 5, 1471–1492, https://doi.org/10.5194/gmd-5-1471-2012, 2012.

He, J., Naik, V., and Horowitz, L. W.: Hydroxyl Radical (OH) Response to Meteorological Forcing and Implication for the Methane Budget, Geophysical Research Letters, 48, https://doi.org/10.1029/2021gl094140, 2021.

He, M., Jacob, D. J., Estrada, L. A., Varon, D. J., Sulprizio, M., Balasus, N., East, J. D., Penn, E., Pendergrass, D. C., Chen, Z., Mooring, T. A., Maasakkers, J. D., Brodrick, P. G., Frankenberg, C., Bowman, K. W., and Bruhwiler, L.: Attributing 2019–2024 methane growth using TROPOMI satellite observations, Science Advances, 12, https://doi.org/10.1126/sciadv.adz9007, 2026.

Hersbach, H., Bell, B., Berrisford, P., Hirahara, S., Horányi, A., Muñoz-Sabater, J., Nicolas, J., Peubey, C., Radu, R., Schepers, D., Simmons, A., Soci, C., Abdalla, S., Abellan, X., Balsamo, G., Bechtold, P., Biavati, G., Bidlot, J., Bonavita, M., De Chiara, G., Dahlgren, P., Dee, D., Diamantakis, M., Dragani, R., Flemming, J., Forbes, R., Fuentes, M., Geer, A., Haimberger, L., Healy, S., Hogan, R. J., Hólm, E., Janisková, M., Keeley, S., Laloyaux, P., Lopez, P., Lupu, C., Radnoti, G., de Rosnay, P., Rozum, I., Vamborg, F., Villaume, S., and Thépaut, J.: The ERA5 global reanalysis, Quarterly Journal of the Royal Meteorological Society, 146, 1999–2049, https://doi.org/10.1002/qj.3803, 2020.

https://doi.org/10.5194/egusphere-2026-4883
Preprint. Discussion started: 14 August 2026

Hodson, E. L., Poulter, B., Zimmermann, N. E., Prigent, C., and Kaplan, J. O.: The El Niño-Southern Oscillation and wetland methane interannual variability, Geophysical Research Letters, 38, n/a–n/a, https://doi.org/10.1029/2011gl046861, 2011.

Hoesly, R., Smith, S., Ahsan, H., Prime, N., O'Rourke, P., Crippa, M., Klimont, Z., Guizzardi, D., Feng, L., Harkins, C., MCDONALD, B., and Wang, S.: CEDS v_2025_04_18 Gridded Emissions Data 0.5 degree, https://doi.org/10.5281/ZENODO.15127477, 2025.

Hoesly, R. M., Smith, S. J., Feng, L., Klimont, Z., Janssens-Maenhout, G., Pitkanen, T., Seibert, J. J., Vu, L., Andres, R. J., Bolt, R. M., Bond, T. C., Dawidowski, L., Kholod, N., ichi Kurokawa, J., Li, M., Liu, L., Lu, Z., Moura, M. C. P., O'Rourke, P. R., and Zhang, Q.: Historical (1750–2014) anthropogenic emissions of reactive gases and aerosols from the Community Emissions Data System (CEDS), Geoscientific Model Development, 11, 369–408, https://doi.org/10.5194/gmd-11-369-2018, 2018.

Holmes, C. D., Prather, M. J., Søvde, O. A., and Myhre, G.: Future methane hydroxyl and their uncertainties: key climate and emission parameters for future predictions, Atmospheric Chemistry and Physics, 13, 285–302, https://doi.org/10.5194/acp-13-285-2013, 2013.

Inness, A., Aben, I., Ades, M., Borsdorff, T., Flemming, J., Jones, L., Landgraf, J., Langerock, B., Nedelec, P., Parrington, M., and Ribas, R.: Assimilation of S5P/TROPOMI carbon monoxide data with the global CAMS near-real-time system, Atmospheric Chemistry and Physics, 22, 14 355–14 376, https://doi.org/10.5194/acp-22-14355-2022, 2022.

Jacob, D. J., Varon, D. J., Cusworth, D. H., Dennison, P. E., Frankenberg, C., Gautam, R., Guanter, L., Kelley, J., McKeever, J., Ott, L. E., Poulter, B., Qu, Z., Thorpe, A. K., Worden, J. R., and Duren, R. M.: Quantifying methane emissions from the global scale down to point sources using satellite observations of atmospheric methane, Atmospheric Chemistry and Physics, 22, 9617–9646, https://doi.org/10.5194/acp-22-9617-2022, 2022.

Kuze, A., Suto, H., Nakajima, M., and Hamazaki, T.: Thermal and near infrared sensor for carbon observation Fourier-transform spectrometer on the Greenhouse Gases Observing Satellite for greenhouse gases monitoring, Applied Optics, 48, 6716, https://doi.org/10.1364/ao.48.006716, 2009.

Lan, X., Basu, S., Schwietzke, S., Bruhwiler, L. M. P., Dlugokencky, E. J., Michel, S. E., Sherwood, O. A., Tans, P. P., Thoning, K., Etiope, G., Zhuang, Q., Liu, L., Oh, Y., Miller, J. B., Pétron, G., Vaughn, B. H., and Crippa, M.: Improved Constraints on Global Methane Emissions and Sinks Using δ13C-CH4, Global Biogeochemical Cycles, 35, https://doi.org/10.1029/2021gb007000, 2021a.

Lan, X., Nisbet, E. G., Dlugokencky, E. J., and Michel, S. E.: What do we know about the global methane budget? Results from four decades of atmospheric CH_4 observations and the way forward, Philosophical Transactions of the Royal Society A: Mathematical, Physical and Engineering Sciences, 379, 20200 440, https://doi.org/10.1098/rsta.2020.0440, 2021b.

Lan, X., Thoning, K., and Dlugokencky, E.: Trends in globally-averaged CH4, N2O, and SF6 determined from NOAA Global Monitoring Laboratory measurements, https://doi.org/10.15138/P8XG-AA10, 2022.

Lan, X., Tans, P., Thoning, K., and NOAA Global Monitoring Laboratory: NOAA Greenhouse Gas Marine Boundary Layer Reference - CH4., https://doi.org/10.15138/DVNP-F961, 2023.

Lawrence, M. G., Jöckel, P., and von Kuhlmann, R.: What does the global mean OH concentration tell us?, Atmospheric Chemistry and Physics, 1, 37–49, https://doi.org/10.5194/acp-1-37-2001, 2001.

Lelieveld, J., Crutzen, P. J., and Dentener, F. J.: Changing concentration, lifetime and climate forcing of atmospheric methane, Tellus B: Chemical and Physical Meteorology, 50, 128, https://doi.org/10.3402/tellusb.v50i2.16030, 1998.

Lelieveld, J., Peters, W., Dentener, F. J., and Krol, M. C.: Stability of tropospheric hydroxyl chemistry, Journal of Geophysical Research: Atmospheres, 107, https://doi.org/10.1029/2002jd002272, 2002.

Lelieveld, J., Gromov, S., Pozzer, A., and Taraborrelli, D.: Global tropospheric hydroxyl distribution budget and reactivity, Atmospheric Chemistry and Physics, 16, 12 477–12 493, https://doi.org/10.5194/acp-16-12477-2016, 2016.

https://doi.org/10.5194/egusphere-2026-4883
Preprint. Discussion started: 14 August 2026

Levy, H.: Normal Atmosphere: Large Radical and Formaldehyde Concentrations Predicted, Science, 173, 141–143, https://doi.org/10.1126/science.173.3992.141, 1971.

Li, H., Ciais, P., Kumar, P., Hauglustaine, D. A., Chevallier, F., Broquet, G., Millet, D. B., Wells, K. C., Lian, J., and Zheng, B.: Global biogenic isoprene emissions 2013–2020 inferred from satellite isoprene observations, Earth System Science Data, 17, 7035–7054, https://doi.org/10.5194/essd-17-7035-2025, 2025.

Libonati, R., Pereira, J. M. C., Da Camara, C. C., Peres, L. F., Oom, D., Rodrigues, J. A., Santos, F. L. M., Trigo, R. M., Gouveia, C. M. P., Machado-Silva, F., Enrich-Prast, A., and Silva, J. M. N.: Twenty-first century droughts have not increasingly exacerbated fire season severity in the Brazilian Amazon, Scientific Reports, 11, https://doi.org/10.1038/s41598-021-82158-8, 2021.

Logan, J. A., Prather, M. J., Wofsy, S. C., and McElroy, M. B.: Tropospheric chemistry: A global perspective, Journal of Geophysical Research: Oceans, 86, 7210–7254, https://doi.org/10.1029/jc086ic08p07210, 1981.

Lorente, A., Borsdorff, T., Butz, A., Hasekamp, O., aan de Brugh, J., Schneider, A., Wu, L., Hase, F., Kivi, R., Wunch, D., Pollard, D. F., Shiomi, K., Deutscher, N. M., Velazco, V. A., Roehl, C. M., Wennberg, P. O., Warneke, T., and Landgraf, J.: Methane retrieved from TROPOMI: improvement of the data product and validation of the first 2 years of measurements, Atmospheric Measurement Techniques, 14, 665–684, https://doi.org/10.5194/amt-14-665-2021, 2021.

Martínez-Alonso, S., Deeter, M., Worden, H., Borsdorff, T., Aben, I., Commane, R., Daube, B., Francis, G., George, M., Landgraf, J., Mao, D., McKain, K., and Wofsy, S.: 1.5 years of TROPOMI CO measurements: comparisons to MOPITT and ATom, Atmospheric Measurement Techniques, 13, 4841–4864, https://doi.org/10.5194/amt-13-4841-2020, 2020.

Masarie, K. A. and Tans, P. P.: Extension and integration of atmospheric carbon dioxide data into a globally consistent measurement record, Journal of Geophysical Research, 100, 11 593, https://doi.org/10.1029/95jd00859, 1995.

McKain, K. and Sweeney, C.: ATom: CO_2 CH_4 and CO Measurements from Picarro 2016-2018, https://doi.org/10.3334/ORNLDAAC/1732, 2021.

Meinshausen, M., Vogel, E., Nauels, A., Lorbacher, K., Meinshausen, N., Etheridge, D. M., Fraser, P. J., Montzka, S. A., Rayner, P. J., Trudinger, C. M., Krummel, P. B., Beyerle, U., Canadell, J. G., Daniel, J. S., Enting, I. G., Law, R. M., Lunder, C. R., O'Doherty, S., Prinn, R. G., Reimann, S., Rubino, M., Velders, G. J. M., Vollmer, M. K., Wang, R. H. J., and Weiss, R.: Historical greenhouse gas concentrations for climate modelling (CMIP6), Geoscientific Model Development, 10, 2057–2116, https://doi.org/10.5194/gmd-10-2057-2017, 2017.

Michel, S. E., Lan, X., Miller, J., Tans, P., Clark, J. R., Schaefer, H., Sperlich, P., Brailsford, G., Morimoto, S., Moossen, H., and Li, J.: Rapid shift in methane carbon isotopes suggests microbial emissions drove record high atmospheric methane growth in 2020–2022, Proceedings of the National Academy of Sciences, 121, https://doi.org/10.1073/pnas.2411212121, 2024.

Mirrezaei, M. A., Gaubert, B., Arellano, A. F., Fernandez, R. P., Ortega, I., Emmons, L. K., Kinnison, D., Roozitalab, B., McKain, K., Bruhwiler, L., Oh, Y., Saiz-Lopez, A., Cuevas, C. A., Feng, C., Xu, Y., and Brasseur, G. P.: Toward Realistic Prognostic Modeling of the Methane Chemical Loss, Journal of Geophysical Research: Atmospheres, 131, https://doi.org/10.1029/2025jd045079, 2025.

Miyazaki, K., Sekiya, T., Fu, D., Bowman, K. W., Kulawik, S. S., Sudo, K., Walker, T., Kanaya, Y., Takigawa, M., Ogochi, K., Eskes, H., Boersma, K. F., Thompson, A. M., Gaubert, B., Barre, J., and Emmons, L. K.: Balance of Emission and Dynamical Controls on Ozone During the Korea-United States Air Quality Campaign From Multiconstituent Satellite Data Assimilation, Journal of Geophysical Research: Atmospheres, 124, 387–413, https://doi.org/10.1029/2018jd028912, 2019.

https://doi.org/10.5194/egusphere-2026-4883
Preprint. Discussion started: 14 August 2026

Miyazaki, K., Bowman, K., Sekiya, T., Takigawa, M., Neu, J. L., Sudo, K., Osterman, G., and Eskes, H.: Global tropospheric ozone responses to reduced NO_x emissions linked to the COVID-19 worldwide lockdowns, Science Advances, 7, https://doi.org/10.1126/sciadv.abf7460, 2021.

Montzka, S. A., Krol, M., Dlugokencky, E., Hall, B., Jöckel, P., and Lelieveld, J.: Small Interannual Variability of Global Atmospheric Hydroxyl, Science, 331, 67–69, https://doi.org/10.1126/science.1197640, 2011.

Morgenstern, O., Moss, R., Manning, M., Zeng, G., Schaefer, H., Usoskin, I., Turnbull, J., Brailsford, G., Nichol, S., and Bromley, T.: Radiocarbon monoxide indicates increasing atmospheric oxidizing capacity, Nature Communications, 16, https://doi.org/10.1038/s41467-024-55603-1, 2025.

Murray, L. T., Logan, J. A., and Jacob, D. J.: Interannual variability in tropical tropospheric ozone and OH: The role of lightning, Journal of Geophysical Research: Atmospheres, 118, https://doi.org/10.1002/jgrd.50857, 2013.

Murray, L. T., Fiore, A. M., Shindell, D. T., Naik, V., and Horowitz, L. W.: Large uncertainties in global hydroxyl projections tied to fate of reactive nitrogen and carbon, Proceedings of the National Academy of Sciences, 118, https://doi.org/10.1073/pnas.2115204118, 2021.

Müller, J.-F., Liu, Z., Nguyen, V. S., Stavrakou, T., Harvey, J. N., and Peeters, J.: The reaction of methyl peroxy and hydroxyl radicals as a major source of atmospheric methanol, Nature Communications, 7, https://doi.org/10.1038/ncomms13213, 2016.

Naik, V., Voulgarakis, A., Fiore, A. M., Horowitz, L. W., Lamarque, J.-F., Lin, M., Prather, M. J., Young, P. J., Bergmann, D., Cameron-Smith, P. J., Cionni, I., Collins, W. J., Dalsøren, S. B., Doherty, R., Eyring, V., Faluvegi, G., Folberth, G. A., Josse, B., Lee, Y. H., MacKenzie, I. A., Nagashima, T., van Noije, T. P. C., Plummer, D. A., Righi, M., Rumbold, S. T., Skeie, R., Shindell, D. T., Stevenson, D. S., Strode, S., Sudo, K., Szopa, S., and Zeng, G.: Preindustrial to present-day changes in tropospheric hydroxyl radical and methane lifetime from the Atmospheric Chemistry and Climate Model Intercomparison Project (ACCMIP), Atmospheric Chemistry and Physics, 13, 5277–5298, https://doi.org/10.5194/acp-13-5277-2013, 2013.

Naus, S., Montzka, S. A., Pandey, S., Basu, S., Dlugokencky, E. J., and Krol, M.: Constraints and biases in a tropospheric two-box model of OH, Atmospheric Chemistry and Physics, 19, 407–424, https://doi.org/10.5194/acp-19-407-2019, 2019.

Nicely, J. M., Canty, T. P., Manyin, M., Oman, L. D., Salawitch, R. J., Steenrod, S. D., Strahan, S. E., and Strode, S. A.: Changes in Global Tropospheric OH Expected as a Result of Climate Change Over the Last Several Decades, Journal of Geophysical Research: Atmospheres, 123, https://doi.org/10.1029/2018jd028388, 2018.

Nisbet, E. G. and Manning, M. R.: What is causing the methane surge?, Science, 391, 556–557, https://doi.org/10.1126/science.aee6226, 2026.

Nisbet, E. G., Manning, M. R., Dlugokencky, E. J., Fisher, R. E., Lowry, D., Michel, S. E., Myhre, C. L., Platt, S. M., Allen, G., Bousquet, P., Brownlow, R., Cain, M., France, J. L., Hermansen, O., Hossaini, R., Jones, A. E., Levin, I., Manning, A. C., Myhre, G., Pyle, J. A., Vaughn, B. H., Warwick, N. J., and White, J. W. C.: Very Strong Atmospheric Methane Growth in the 4 Years 2014-2017: Implications for the Paris Agreement, Global Biogeochemical Cycles, 33, 318–342, https://doi.org/10.1029/2018gb006009, 2019.

Nisbet, E. G., Manning, M. R., Dlugokencky, E. J., Michel, S. E., Lan, X., Röckmann, T., Denier van der Gon, H. A. C., Schmitt, J., Palmer, P. I., Dyonisius, M. N., Oh, Y., Fisher, R. E., Lowry, D., France, J. L., White, J. W. C., Brailsford, G., and Bromley, T.: Atmospheric Methane: Comparison Between Methane's Record in 2006–2022 and During Glacial Terminations, Global Biogeochemical Cycles, 37, https://doi.org/10.1029/2023gb007875, 2023.

Oh, Y., Zhuang, Q., Welp, L. R., Liu, L., Lan, X., Basu, S., Dlugokencky, E. J., Bruhwiler, L., Miller, J. B., Michel, S. E., Schwietzke, S., Tans, P., Ciais, P., and Chanton, J. P.: Improved global wetland carbon isotopic signatures support post-2006 microbial methane emission increase, Communications Earth & Environment, 3, https://doi.org/10.1038/s43247-022-00488-5, 2022.

https://doi.org/10.5194/egusphere-2026-4883
Preprint. Discussion started: 14 August 2026

Oh, Y., Bruhwiler, L., Lan, X., Schuldt, K., Basu, S., Thoning, K., Michel, S. E., Clark, R., Miller, J. B., Andrews, A., Aalto, T., Andrade, M., Aoki, S., Apadula, F., Arduini, J., Arnold, S., Baier, B., Bäni, L., Bartyzel, J., Bentz, G., Biermann, T., Biraud, S. C., Blanc, P.-E., Boenisch, H., Brailsford, G., Brand, W. A., Brunner, D., Bui, T. P. V., Bulk, P. v. d., Burban, B., Calzolari, F., Chang, C. S., Chen, H., Chmura, L., Choi, Y., Clair, J. M. S., Climadat, S., Coletta, J. D., Colomb, A., Condori, L., Conen, F., Conil, S., Couret, C., Crippa, M., Cristofanelli, P., Cuevas, E., Curcoll, R., Daube, B., Davis, K. J., Dean-Day, J. M., Delmotte, M., Desai, A., DiGangi, E., Diskin, G. S., DiGangi, J. P., Elsasser, M., Emmenegger, L., Esenzhanova, G., Etiope, G., Fischer, M. L., Forster, G., Frumau, A., Fuente-Lastra, M., Fujita, R., Galkowski, M., Gatti, L. V., Gehrlein, T., Gerbig, C., Gheusi, F., Gloor, E., Goto, D., Hammer, S., Hanisco, T. F., Haszpra, L., Hatakka, J., Heimann, M., Heliasz, M., Heltai, D., Henne, S., Hensen, A., Hermans, C., Hermansen, O., Hoheisel, A., Holst, J., Iorio, T. D., Iraci, L. T., Ivakhov, V., Jaffe, D. A., Jordan, A., Joubert, W., Kang, H.-Y., Karion, A., Kazan, V., Keeling, R. F., Keronen, P., Kers, B., Kim, J., Klausen, J., Kneuer, T., Ko, M.-Y., Kolari, P., Kominkova, K., Kort, E., Kozlova, E., Krummel, P. B., Kubistin, D., Kulawik, S. S., Kumps, N., Labuschagne, C., Langenfelds, R. L., Lanza, A., Larmanou, E., Laurent, O., Laurila, T., Lauvaux, T., Lavric, J., Lee, C.-H., Lee, S., Lee, H., Lee, J., Lehner, I., Lehtinen, K., Leppert, R., Leskinen, A., Leuenberger, M., Levin, I., Levula, J., Lindauer, M., Löfvenius, M. O., Loh, Z. M., Lopez, M., Lowry, D., Lueker, T. J., Lunder, C. R., Machida, T., Mammarella, I., Manca, G., Manning, A., Marek, M. V., Marklund, P., Marrero, J. E., Martin, M. Y., Martin, D., Martins, G. A., Matsueda, H., Mazière, M. D., McKain, K., Meinhardt, F., Menoud, M., Metzger, J.-M., Mihalopoulos, N., Miles, N. L., Miller, C. E., Mölder, M., Monteiro, V., Montzka, S., Moore, F., Moossen, H., Moreno, C., Morgan, E., Morgui, J.-A., Morimoto, S., Müller-Williams, J., Mutuku, M., Myhre, C. L., Necki, J., Nichol, S., Nisbet, E., Niwa, Y., Njiru, D. M., Noe, S. M., Obersteiner, F., ODoherty, S., Paramonova, N., Parworth, C. L., Peltola, O., Philippon, C., Piacentino, S., Pichon, J. M., Pickers, P., Pitt, J., Pittman, J., Plass-Dülmer, C., Platt, S. M., Popa, M. E., Pouter, B., Prinzivalli, S., Ramonet, M., Randerson, J., Richardson, S. J., Ries, L., Rigouleau, L.-J., Rivas, P. P., Röckmann, T., Rothe, M., Ryoo, J.-M., Santoni, G., Sarra, A. G. d., Sasakawa, M., Scheeren, B., Schmidt, M., Schuck, T., Schumacher, M., Seifert, T., Sha, M. K., Shepson, P., Sherwood, O., Shin, D., Sloop, C. D., Smale, D., Smith, P. D., Sørensen, L. L., Souza, R. A. F. d., Spain, G., Stanley, K. M., Steger, D., Steinbacher, M., Stephens, B., Sweeney, C., Taipale, R., Takatsuji, S., Thoning, K., Timas, H., Torres, G., Trisolino, P., Turnbull, J., Uhse, K., Umezawa, T., Veen, C. v. d., Vermeulen, A., Viner, B., Vitkova, G., Vries, M. d., Watson, A., Weiss, R., Werf, G. v. d., Weyrauch, D., Wofsy, S. C., Worsey, J., Worthy, D., Xueref-Remy, I., Yates, E. L., Young, D., Yver-Kwok, C., Zaehle, S., Zahn, A., Zazzeri, G., Zellweger, C., Zhang, Z., and Zimnoch, M.: CarbonTracker CH4 2025, https://doi.org/10.25925/HXKS-V755, 2025.

Oh, Y., Bruhwiler, L., Lan, X., Halder, S., Riddell-Young, B., Basu, S., Miller, J. B., Michel, S., Schuldt, K., Andrews, A., Biraud, S., Chmura, L., lorio, T. D., Guerette, E.-A., Kozlova, E., Liu, L., Montaguti, S., Morimoto, S., Steinbacher, M., Umezawa, T., Xueref-Remy, I., and Zazzeri, G.: Isotopic constraints in methane inversions reveal larger trends in wetland emissions with improved linkage to terrestrial water storage, Nature Communications, https://doi.org/10.1038/s41467-026-74777-4, 2026.

Ortega, I., Gaubert, B., Hannigan, J. W., Brasseur, G., Worden, H. M., Blumenstock, T., Fu, H., Hase, F., Jeseck, P., Jones, N., Liu, C., Mahieu, E., Morino, I., Murata, I., Notholt, J., Palm, M., Röhling, A., Té, Y., Strong, K., Sun, Y., and Yamanouchi, S.: Anomalies of O3 CO C2H2 H2CO and C2H6 detected with multiple ground-based Fourier-transform infrared spectrometers and assessed with model simulation in 2020: COVID-19 lockdowns versus natural variability, Elem Sci Anth, 11, https://doi.org/10.1525/elementa.2023.00015, 2023.

Ortega, I., Hannigan, J. W., Baier, B. C., McKain, K., and Smale, D.: Advancing CH_4 and N_2O retrieval strategies for NDAC-C/IRWG FTIR observations with the support of airborne in situ measurements, Atmospheric Measurement Techniques, 18, 2353–2371, https://doi.org/10.5194/amt-18-2353-2025, 2025.

https://doi.org/10.5194/egusphere-2026-4883
Preprint. Discussion started: 14 August 2026

Pan, L. L., Atlas, E. L., Honomichl, S. B., Smith, W. P., Kinnison, D. E., Solomon, S., Santee, M. L., Saiz-Lopez, A., Laube, J. C., Wang, B., Ueyama, R., Bresch, J. F., Hornbrook, R. S., Apel, E. C., Hills, A. J., Treadaway, V., Smith, K., Schauffler, S., Donnelly, S., Hendershot, R., Lueb, R., Campos, T., Viciani, S., D'Amato, F., Bianchini, G., Barucci, M., Podolske, J. R., Iraci, L. T., Gurganus, C., Bui, P., Dean-Day, J. M., Millán, L., Ryoo, J.-M., Barletta, B., Koo, J.-H., Kim, J., Liang, Q., Randel, W. J., Thornberry, T., and Newman, P. A.: East Asian summer monsoon delivers large abundances of very short-lived organic chlorine substances to the lower stratosphere, Proceedings of the National Academy of Sciences, 121, https://doi.org/10.1073/pnas.2318716121, 2024.

Parker, R. J. and Boesch, H.: University of Leicester GOSAT Proxy XCH4 v9.0, https://doi.org/10.5285/18EF8247F52A4CB6A14013F8235CC1EB, 2020.

Parker, R. J., Webb, A., Boesch, H., Somkuti, P., Guillo, R. B., Noia, A. D., Kalaitzi, N., Anand, J. S., Bergamaschi, P., Chevallier, F., Palmer, P. I., Feng, L., Deutscher, N. M., Feist, D. G., Griffith, D. W. T., Hase, F., Kivi, R., Morino, I., Notholt, J., Oh, Y.-S., Ohyama, H., Petri, C., Pollard, D. F., Roehl, C., Sha, M. K., Shiomi, K., Strong, K., Sussmann, R., Té, Y., Velazco, V. A., Warneke, T., Wennberg, P. O., and Wunch, D.: A decade of GOSAT Proxy satellite CH_4 observations., Earth System Science Data, 12, 3383–3412, https://doi.org/10.5194/essd-12-3383-2020, 2020.

Patra, P. K., Houweling, S., Krol, M., Bousquet, P., Belikov, D., Bergmann, D., Bian, H., Cameron-Smith, P., Chipperfield, M. P., Corbin, K., Fortems-Cheiney, A., Fraser, A., Gloor, E., Hess, P., Ito, A., Kawa, S. R., Law, R. M., Loh, Z., Maksyutov, S., Meng, L., Palmer, P. I., Prinn, R. G., Rigby, M., Saito, R., and Wilson, C.: TransCom model simulations of CH_4 and related species: linking transport surface flux and chemical loss with CH_4 variability in the troposphere and lower stratosphere, Atmospheric Chemistry and Physics, 11, 12 813–12 837, https://doi.org/10.5194/acp-11-12813-2011, 2011.

Patra, P. K., Krol, M. C., Prinn, R. G., Takigawa, M., Mühle, J., Montzka, S. A., Lal, S., Yamashita, Y., Naus, S., Chandra, N., Weiss, R. F., Krummel, P. B., Fraser, P. J., O'Doherty, S., and Elkins, J. W.: Methyl Chloroform Continues to Constrain the Hydroxyl (OH) Variability in the Troposphere, Journal of Geophysical Research: Atmospheres, 126, https://doi.org/10.1029/2020jd033862, 2021.

Peng, S., Lin, X., Thompson, R. L., Xi, Y., Liu, G., Hauglustaine, D., Lan, X., Poulter, B., Ramonet, M., Saunois, M., Yin, Y., Zhang, Z., Zheng, B., and Ciais, P.: Wetland emission and atmospheric sink changes explain methane growth in 2020, Nature, 612, 477–482, https://doi.org/10.1038/s41586-022-05447-w, 2022.

Prather, M. J., Ehhalt, D., Etheridge, D., Derwent, R., Fraser, P., Hauglustaine, D., Jackels, C., Johns, T., Lal, S., Law, K., Low, J., Mahowald, N., Prinn, R., Pauline, J., Rasmussen, R., Schwarzkopf, M. D., and Stern, D.: Atmospheric Chemistry and Greenhouse Gases, in: Climate Change 2001: The Scientific Basis. Contribution of Working Group I to the Third Assessment Report of the Intergovernmental Panel on Climate Change, edited by Houghton, J. T., Ding, Y., Griggs, D. J., Noguer, M., van der Linden, P. J., Dai, X., Maskell, K., and Johnson, C. A., pp. 239–287, Cambridge University Press, Cambridge, United Kingdom and New York, NY, USA, https://ipcc.ch, 2001.

Prather, M. J., Holmes, C. D., and Hsu, J.: Reactive greenhouse gas scenarios: Systematic exploration of uncertainties and the role of atmospheric chemistry, Geophysical Research Letters, 39, n/a–n/a, https://doi.org/10.1029/2012gl051440, 2012.

Price, P., Bottorff, B., Jenkins, J., Brune, W. H., and Stevens, P. S.: Re-assessing hydroxyl radical chemistry in the atmosphere: Instrument interferences may explain previous measurement discrepancies, Communications Earth amp; Environment, 6, https://doi.org/10.1038/s43247-025-02308-y, 2025.

Prinn, R. G., Huang, J., Weiss, R. F., Cunnold, D. M., Fraser, P. J., Simmonds, P. G., McCulloch, A., Harth, C., Salameh, P., O'Doherty, S., Wang, R. H. J., Porter, L., and Miller, B. R.: Evidence for Substantial Variations of Atmospheric Hydroxyl Radicals in the Past Two Decades, Science, 292, 1882–1888, https://doi.org/10.1126/science.1058673, 2001.

https://doi.org/10.5194/egusphere-2026-4883
Preprint. Discussion started: 14 August 2026

Qu, Z., Jacob, D. J., Zhang, Y., Shen, L., Varon, D. J., Lu, X., Scarpelli, T., Bloom, A., Worden, J., and Parker, R. J.: Attribution of the 2020 surge in atmospheric methane by inverse analysis of GOSAT observations, Environmental Research Letters, 17, 094 003, https://doi.org/10.1088/1748-9326/ac8754, 2022.

Qu, Z., Jacob, D. J., Bloom, A. A., Worden, J. R., Parker, R. J., and Boesch, H.: Inverse modeling of 2010–2022 satellite observations shows that inundation of the wet tropics drove the 2020–2022 methane surge, Proceedings of the National Academy of Sciences, 121, https://doi.org/10.1073/pnas.2402730121, 2024.

Randerson, J., van der Werf, G., Giglio, L., Collatz, G., and Kasibhatla, P.: Global Fire Emissions Database, Version 4.1 (GFEDv4), https://doi.org/10.3334/ORNLDAAC/1293, 2015.

Richter, J. H., Joseph, E., Arcodia, M. C., Berner, J., Demuth, J. L., Falloon, P., Romine, G. S., Cohen, J. T., Gonzalez-Cruz, J., El Gharamti, M., Hoppe, B., Kumar, S., Mariotti, A., Mishra, D., Pegion, K., Pu, Z., Quagraine, K. A., Quagraine, K. T., Roychoudhury, C., Ryan, J., Stone, Z., Das, D., Gaubert, B., Kapnick, S., and Zarzycki, C.: Earth System Predictability Across Time Scales for a Resilient Society: A Research Community Perspective, Bulletin of the American Meteorological Society, https://doi.org/10.1175/bams-d-24-0155.1, 2026.

Riddell-Young, B., Michel, S. E., Lan, X., Tans, P., Röckmann, T., Dasgupta, B., Oh, Y., Bruhwiler, L. M. P., Fujita, R., Umezawa, T., Morimoto, S., and Miller, J. B.: Microbial driver of 2006–2023 CH_4 growth indicated by trends in atmospheric δD–CH_4 and δ^{13}C–CH_4, Proceedings of the National Academy of Sciences, 122, https://doi.org/10.1073/pnas.2516543122, 2025.

Rigby, M., Prinn, R. G., Fraser, P. J., Simmonds, P. G., Langenfelds, R. L., Huang, J., Cunnold, D. M., Steele, L. P., Krummel, P. B., Weiss, R. F., O'Doherty, S., Salameh, P. K., Wang, H. J., Harth, C. M., Mühle, J., and Porter, L. W.: Renewed growth of atmospheric methane, Geophysical Research Letters, 35, https://doi.org/10.1029/2008gl036037, 2008.

Rigby, M., Montzka, S. A., Prinn, R. G., White, J. W. C., Young, D., O'Doherty, S., Lunt, M. F., Ganesan, A. L., Manning, A. J., Simmonds, P. G., Salameh, P. K., Harth, C. M., Mühle, J., Weiss, R. F., Fraser, P. J., Steele, L. P., Krummel, P. B., McCulloch, A., and Park, S.: Role of atmospheric oxidation in recent methane growth, Proceedings of the National Academy of Sciences, 114, 5373–5377, https://doi.org/10.1073/pnas.1616426114, 2017.

Saiz-Lopez, A., Mahajan, A. S., Abbatt, J., Bobrowski, N., Brown, S. S., Burrows, J. P., Carpenter, L. J., Chipperfield, M. P., Cuevas, C. A., Fernandez, R. P., Hossaini, R., Kinnison, D. E., Lamarque, J.-F., Finlayson-Pitts, B. J., Plane, J. M. C., Platt, U., Pratt, K. A., Ravishankara, A. R., Salawitch, R. J., Saltzman, E. S., Simpson, W. R., Solomon, S., Thornton, J. A., and Wang, T.: The influence of short-lived halogens on atmospheric chemistry and climate, Nature, 648, 289–299, https://doi.org/10.1038/s41586-025-09753-x, 2025.

Santoni, G. W., Daube, B. C., Kort, E. A., Jiménez, R., Park, S., Pittman, J. V., Gottlieb, E., Xiang, B., Zahniser, M. S., Nelson, D. D., McManus, J. B., Peischl, J., Ryerson, T. B., Holloway, J. S., Andrews, A. E., Sweeney, C., Hall, B., Hintsa, E. J., Moore, F. L., Elkins, J. W., Hurst, D. F., Stephens, B. B., Bent, J., and Wofsy, S. C.: Evaluation of the airborne quantum cascade laser spectrometer (QCLS) measurements of the carbon and greenhouse gas suite – CO_2 CH_4 N_2O and CO – during the CalNex and HIPPO campaigns, Atmospheric Measurement Techniques, 7, 1509–1526, https://doi.org/10.5194/amt-7-1509-2014, 2014.

Saunois, M., Martinez, A., Poulter, B., Zhang, Z., Raymond, P. A., Regnier, P., Canadell, J. G., Jackson, R. B., Patra, P. K., Bousquet, P., Ciais, P., Dlugokencky, E. J., Lan, X., Allen, G. H., Bastviken, D., Beerling, D. J., Belikov, D. A., Blake, D. R., Castaldi, S., Crippa, M., Deemer, B. R., Dennison, F., Etiope, G., Gedney, N., Höglund-Isaksson, L., Holgerson, M. A., Hopcroft, P. O., Hugelius, G., Ito, A., Jain, A. K., Janardanan, R., Johnson, M. S., Kleinen, T., Krummel, P. B., Lauerwald, R., Li, T., Liu, X., McDonald, K. C., Melton, J. R., Mühle, J., Müller, J., Murguia-Flores, F., Niwa, Y., Noce, S., Pan, S., Parker, R. J., Peng, C., Ramonet, M., Riley, W. J., Rocher-Ros, G., Rosentreter, J. A., Sasakawa, M., Segers, A., Smith, S. J., Stanley, E. H., Thanwerdas, J., Tian, H., Tsuruta, A., Tubiello, F. N., Weber,

https://doi.org/10.5194/egusphere-2026-4883
Preprint. Discussion started: 14 August 2026

T. S., van der Werf, G. R., Worthy, D. E. J., Xi, Y., Yoshida, Y., Zhang, W., Zheng, B., Zhu, Q., Zhu, Q., and Zhuang, Q.: Global Methane Budget 2000–2020, Earth System Science Data, 17, 1873–1958, https://doi.org/10.5194/essd-17-1873-2025, 2025.

Sfendla, Y., Stavrakou, T., Müller, J.-F., Oomen, G.-M., Opacka, B., Danckaert, T., De Smedt, I., and Lerot, C.: Global VOC emissions quantified from inversion of TROPOMI spaceborne formaldehyde and glyoxal data, Atmospheric Chemistry and Physics, 26, 733–767, https://doi.org/10.5194/acp-26-733-2026, 2026.

Shindell, D. T., Faluvegi, G., Bell, N., and Schmidt, G. A.: An emissions-based view of climate forcing by methane and tropospheric ozone, Geophysical Research Letters, 32, https://doi.org/10.1029/2004gl021900, 2005.

Shindell, D. T., Sadavarte, P., Aben, I., Bredariol, T. d. O., Dreyfus, G., Höglund-Isaksson, L., Poulter, B., Saunois, M., Schmidt, G. A., Szopa, S., Rentz, K., Parsons, L., Qu, Z., Faluvegi, G., and Maasakkers, J. D.: The methane imperative, Frontiers in Science, 2, https://doi.org/10.3389/fsci.2024.1349770, 2024.

Shutter, J. D., Millet, D. B., Wells, K. C., Payne, V. H., Nowlan, C. R., and Abad, G. G.: Interannual changes in atmospheric oxidation over forests determined from space, Science Advances, 10, https://doi.org/10.1126/sciadv.adn1115, 2024.

Sindelarova, K., Markova, J., Simpson, D., Huszar, P., Karlicky, J., Darras, S., and Granier, C.: High-resolution biogenic global emission inventory for the time period 2000–2019 for air quality modelling, Earth System Science Data, 14, 251–270, https://doi.org/10.5194/essd-14-251-2022, 2022.

Soulie, A., Granier, C., Darras, S., Zilbermann, N., Doumbia, T., Guevara, M., Jalkanen, J.-P., Keita, S., Liousse, C., Crippa, M., Guizzardi, D., Hoesly, R., and Smith, S. J.: Global anthropogenic emissions (CAMS-GLOB-ANT) for the Copernicus Atmosphere Monitoring Service simulations of air quality forecasts and reanalyses, Earth System Science Data, 16, 2261–2279, https://doi.org/10.5194/essd-16-2261-2024, 2024.

Souri, A. H., Duncan, B. N., Strode, S. A., Anderson, D. C., Manyin, M. E., Liu, J., Oman, L. D., Zhang, Z., and Weir, B.: Enhancing long-term trend simulation of the global tropospheric hydroxyl (TOH) and its drivers from 2005 to 2019: a synergistic integration of model simulations and satellite observations, Atmospheric Chemistry and Physics, 24, 8677–8701, https://doi.org/10.5194/acp-24-8677-2024, 2024.

Staniaszek, Z., Griffiths, P. T., Folberth, G. A., O'Connor, F. M., Abraham, N. L., and Archibald, A. T.: The role of future anthropogenic methane emissions in air quality and climate, npj Climate and Atmospheric Science, 5, https://doi.org/10.1038/s41612-022-00247-5, 2022.

Stevenson, D. S., Zhao, A., Naik, V., O'Connor, F. M., Tilmes, S., Zeng, G., Murray, L. T., Collins, W. J., Griffiths, P. T., Shim, S., Horowitz, L. W., Sentman, L. T., and Emmons, L.: Trends in global tropospheric hydroxyl radical and methane lifetime since 1850 from AerChem-MIP, Atmospheric Chemistry and Physics, 20, 12 905–12 920, https://doi.org/10.5194/acp-20-12905-2020, 2020.

Stevenson, D. S., Derwent, R. G., Wild, O., and Collins, W. J.: COVID-19 lockdown emission reductions have the potential to explain over half of the coincident increase in global atmospheric methane, Atmospheric Chemistry and Physics, 22, 14 243–14 252, https://doi.org/10.5194/acp-22-14243-2022, 2022.

Strode, S., Duncan, B., Anderson, D., Oman, L. D., Orbe, C., Deushi, M., Jöckel, P., and Manyin, M.: The Predictive Power of Combining Chemical and Dynamical Variables for Explaining the OH Distribution and Spatiotemporal Variability, Journal of Geophysical Research: Atmospheres, 131, https://doi.org/10.1029/2025jd044363, 2026.

Szopa, S., Naik, V., Adhikary, B., Artaxo, P., Berntsen, T., Collins, W., Fuzzi, S., Gallardo, L., Kiendler-Scharr, A., Klimont, Z., Liao, H., Unger, N., and Zanis, P.: Short-Lived Climate Forcers, chap. Contribution of Working Group I to the Sixth Assessment Report of the Intergovernmental Panel on Climate Change, p. 817–922, Contribution of Working Group I to the Sixth Assessment Report of the Intergovernmental Panel on Climate Change, Cambridge University Press, https://doi.org/10.1017/9781009157896.008, 2021.

https://doi.org/10.5194/egusphere-2026-4883
Preprint. Discussion started: 14 August 2026

Tan, Z., Ma, X., Lu, K., Li, X., Zhu, Q., Rohrer, F., Novelli, A., Fuchs, H., Wahner, A., Whalley, L., Heard, D., Brown, S., Zhang, X., and Zhang, Y.: Governing atmospheric oxidation capacity is the key to synergistic air quality and climate gains, One Earth, 9, 101 569, https://doi.org/10.1016/j.oneear.2025.101569, 2026.

Tang, Z., Yang, P., Miyazaki, K., Worden, J., Worden, H., Henze, D. K., Jones, D. B. A., and Jiang, Z.: Global CO emissions and drivers of atmospheric CO trends constrained by MOPITT satellite measurements, Atmospheric Chemistry and Physics, 26, 5531–5551, https://doi.org/10.5194/acp-26-5531-2026, 2026.

Thompson, A. M.: The Oxidizing Capacity of the Earth's Atmosphere: Probable Past and Future Changes, Science, 256, 1157–1165, https://doi.org/10.1126/science.256.5060.1157, 1992.

Thompson, C. R., Wofsy, S. C., Prather, M. J., Newman, P. A., Hanisco, T. F., Ryerson, T. B., Fahey, D. W., Apel, E. C., Brock, C. A., Brune, W. H., Froyd, K., Katich, J. M., Nicely, J. M., Peischl, J., Ray, E., Veres, P. R., Wang, S., Allen, H. M., Asher, E., Bian, H., Blake, D., Bourgeois, I., Budney, J., Bui, T. P., Butler, A., Campuzano-Jost, P., Chang, C., Chin, M., Commane, R., Correa, G., Crounse, J. D., Daube, B., Dibb, J. E., DiGangi, J. P., Diskin, G. S., Dollner, M., Elkins, J. W., Fiore, A. M., Flynn, C. M., Guo, H., Hall, S. R., Hannun, R. A., Hills, A., Hintsa, E. J., Hodzic, A., Hornbrook, R. S., Huey, L. G., Jimenez, J. L., Keeling, R. F., Kim, M. J., Kupc, A., Lacey, F., Lait, L. R., Lamarque, J.-F., Liu, J., McKain, K., Meinardi, S., Miller, D. O., Montzka, S. A., Moore, F. L., Morgan, E. J., Murphy, D. M., Murray, L. T., Nault, B. A., Neuman, J. A., Nguyen, L., Gonzalez, Y., Rollins, A., Rosenlof, K., Sargent, M., Schill, G., Schwarz, J. P., Clair, J. M. S., Steenrod, S. D., Stephens, B. B., Strahan, S. E., Strode, S. A., Sweeney, C., Thames, A. B., Ullmann, K., Wagner, N., Weber, R., Weinzierl, B., Wennberg, P. O., Williamson, C. J., Wolfe, G. M., and Zeng, L.: The NASA Atmospheric Tomography (ATom) Mission: Imaging the Chemistry of the Global Atmosphere, Bulletin of the American Meteorological Society, 103, E761–E790, https://doi.org/10.1175/bams-d-20-0315.1, 2022.

Thompson, R. L., Nisbet, E. G., Pisso, I., Stohl, A., Blake, D., Dlugokencky, E. J., Helmig, D., and White, J. W. C.: Variability in Atmospheric Methane From Fossil Fuel and Microbial Sources Over the Last Three Decades, Geophysical Research Letters, 45, https://doi.org/10.1029/2018gl078127, 2018.

Thompson, R. L., Montzka, S. A., Vollmer, M. K., Arduini, J., Crotwell, M., Krummel, P. B., Lunder, C., Mühle, J., O'Doherty, S., Prinn, R. G., Reimann, S., Vimont, I., Wang, H., Weiss, R. F., and Young, D.: Estimation of the atmospheric hydroxyl radical oxidative capacity using multiple hydrofluorocarbons (HFCs), Atmospheric Chemistry and Physics, 24, 1415–1427, https://doi.org/10.5194/acp-24-1415-2024, 2024.

Travis, K. R., Heald, C. L., Allen, H. M., Apel, E. C., Arnold, S. R., Blake, D. R., Brune, W. H., Chen, X., Commane, R., Crounse, J. D., Daube, B. C., Diskin, G. S., Elkins, J. W., Evans, M. J., Hall, S. R., Hintsa, E. J., Hornbrook, R. S., Kasibhatla, P. S., Kim, M. J., Luo, G., McKain, K., Millet, D. B., Moore, F. L., Peischl, J., Ryerson, T. B., Sherwen, T., Thames, A. B., Ullmann, K., Wang, X., Wennberg, P. O., Wolfe, G. M., and Yu, F.: Constraining remote oxidation capacity with ATom observations, Atmospheric Chemistry and Physics, 20, 7753–7781, https://doi.org/10.5194/acp-20-7753-2020, 2020.

Turner, A. J., Frankenberg, C., Wennberg, P. O., and Jacob, D. J.: Ambiguity in the causes for decadal trends in atmospheric methane and hydroxyl, Proceedings of the National Academy of Sciences, 114, 5367–5372, https://doi.org/10.1073/pnas.1616020114, 2017.

Turner, A. J., Fung, I., Naik, V., Horowitz, L. W., and Cohen, R. C.: Modulation of hydroxyl variability by ENSO in the absence of external forcing, Proceedings of the National Academy of Sciences, 115, 8931–8936, https://doi.org/10.1073/pnas.1807532115, 2018.

Turner, A. J., Frankenberg, C., and Kort, E. A.: Interpreting contemporary trends in atmospheric methane, Proceedings of the National Academy of Sciences, 116, 2805–2813, https://doi.org/10.1073/pnas.1814297116, 2019.

https://doi.org/10.5194/egusphere-2026-4883
Preprint. Discussion started: 14 August 2026

Turnock, S. T., Allen, R. J., Andrews, M., Bauer, S. E., Deushi, M., Emmons, L., Good, P., Horowitz, L., John, J. G., Michou, M., Nabat, P., Naik, V., Neubauer, D., O'Connor, F. M., Olivié, D., Oshima, N., Schulz, M., Sellar, A., Shim, S., Takemura, T., Tilmes, S., Tsigaridis, K., Wu, T., and Zhang, J.: Historical and future changes in air pollutants from CMIP6 models, Atmospheric Chemistry and Physics, 20, 14 547–14 579, https://doi.org/10.5194/acp-20-14547-2020, 2020.

van Marle, M. and Werf, G. v. d.: input4MIPs.CMIP7.DRES.DRES-CMIP-BB4CMIP7-2-0, https://doi.org/10.25981/ESGF.INPUT4MIPS.CMIP7/252404 2025.

van Marle, M. J. E., Kloster, S., Magi, B. I., Marlon, J. R., Daniau, A.-L., Field, R. D., Arneth, A., Forrest, M., Hantson, S., Kehrwald, N. M., Knorr, W., Lasslop, G., Li, F., Mangeon, S., Yue, C., Kaiser, J. W., and van der Werf, G. R.: Historic global biomass burning emissions for CMIP6 (BB4CMIP) based on merging satellite observations with proxies and fire models (1750–2015), Geoscientific Model Development, 10, 3329–3357, https://doi.org/10.5194/gmd-10-3329-2017, 2017.

Veefkind, J., Aben, I., McMullan, K., Förster, H., de Vries, J., Otter, G., Claas, J., Eskes, H., de Haan, J., Kleipool, Q., van Weele, M., Hasekamp, O., Hoogeveen, R., Landgraf, J., Snel, R., Tol, P., Ingmann, P., Voors, R., Kruizinga, B., Vink, R., Visser, H., and Levelt, P.: TROPOMI on the ESA Sentinel-5 Precursor: A GMES mission for global observations of the atmospheric composition for climate air quality and ozone layer applications, Remote Sensing of Environment, 120, 70–83, https://doi.org/10.1016/j.rse.2011.09.027, 2012.

Wiedinmyer, C., Kimura, Y., McDonald-Buller, E. C., Emmons, L. K., Buchholz, R. R., Tang, W., Seto, K., Joseph, M. B., Barsanti, K. C., Carlton, A. G., and Yokelson, R.: The Fire Inventory from NCAR version 2.5: an updated global fire emissions model for climate and chemistry applications, Geoscientific Model Development, 16, 3873–3891, https://doi.org/10.5194/gmd-16-3873-2023, 2023.

Wild, O. and Ryan, E. M.: Quantifying and addressing the uncertainties in tropospheric ozone and OH in a global chemistry transport model, Atmospheric Chemistry and Physics, 26, 2255–2273, https://doi.org/10.5194/acp-26-2255-2026, 2026.

Wofsy, S. C.: HIAPER Pole-to-Pole Observations (HIPPO): fine-grained global-scale measurements of climatically important atmospheric gases and aerosols, Philosophical Transactions of the Royal Society A: Mathematical Physical and Engineering Sciences, 369, 2073–2086, https://doi.org/10.1098/rsta.2010.0313, 2011.

Wolter, K. and Timlin, M. S.: El Niño/Southern Oscillation behaviour since 1871 as diagnosed in an extended multivariate ENSO index (MEI.ext), International Journal of Climatology, 31, 1074–1087, https://doi.org/10.1002/joc.2336, 2011.

Worden, H. M., Deeter, M. N., Edwards, D. P., Gille, J. C., Drummond, J. R., and Nédélec, P.: Observations of near-surface carbon monoxide from space using MOPITT multispectral retrievals, Journal of Geophysical Research, 115, https://doi.org/10.1029/2010jd014242, 2010.

Worden, J. R., Pandey, S., Zhang, Y., Cusworth, D. H., Qu, Z., Bloom, A. A., Ma, S., Maasakkers, J. D., Byrne, B., Duren, R., Crisp, D., Gordon, D., and Jacob, D. J.: Verifying Methane Inventories and Trends With Atmospheric Methane Data, AGU Advances, 4, https://doi.org/10.1029/2023av000871, 2023.

Xiao, H., Song, C., Li, S., Lu, X., Liang, M., Xia, X., and Yuan, W.: Global Wetland Methane Emissions From 2001 to 2020: Magnitude, Dynamics and Controls, Earth's Future, 12, https://doi.org/10.1029/2024ef004794, 2024.

Yan, C., Kocevska, S., and Krasnoperov, L. N.: Kinetics of the Reaction of CH_3O_2 Radicals with OH Studied over the 292–526 K Temperature Range, The Journal of Physical Chemistry A, 120, 6111–6121, https://doi.org/10.1021/acs.jpca.6b04213, 2016.

Yang, L. H., Jacob, D. J., Lin, H., Dang, R., Bates, K. H., East, J. D., Travis, K. R., Pendergrass, D. C., and Murray, L. T.: Assessment of Hydrogen's Climate Impact Is Affected by Model OH Biases, Geophysical Research Letters, 52, https://doi.org/10.1029/2024gl112445, 2025.

https://doi.org/10.5194/egusphere-2026-4883
Preprint. Discussion started: 14 August 2026

Yin, Y., Ciais, P., Chevallier, F., van der Werf, G. R., Fanin, T., Broquet, G., Boesch, H., Cozic, A., Hauglustaine, D., Szopa, S., and Wang, Y.: Variability of fire carbon emissions in equatorial Asia and its nonlinear sensitivity to El Niño, Geophysical Research Letters, 43, https://doi.org/10.1002/2016gl070971, 2016.

Yin, Y., Chevallier, F., Ciais, P., Bousquet, P., Saunois, M., Zheng, B., Worden, J., Bloom, A. A., Parker, R. J., Jacob, D. J., Dlugokencky, E. J., and Frankenberg, C.: Accelerating methane growth rate from 2010 to 2017: leading contributions from the tropics and East Asia, Atmospheric Chemistry and Physics, 21, 12 631–12 647, https://doi.org/10.5194/acp-21-12631-2021, 2021.

Yoon, J. Y. S., Wells, K. C., Millet, D. B., Swann, A. L. S., Thornton, J., and Turner, A. J.: Impacts of Interannual Isoprene Variations on Methane Lifetimes and Trends, Geophysical Research Letters, 52, https://doi.org/10.1029/2025gl114712, 2025.

Yu, X., Fiore, A. M., Santer, B. D., Correa, G. P., Lamarque, J.-F., Ziemke, J. R., Eastham, S. D., and Zhu, Q.: Anthropogenic Fingerprint Detectable in Upper Tropospheric Ozone Trends Retrieved from Satellite, Environmental Science & Technology, 58, 14 306–14 317, https://doi.org/10.1021/acs.est.4c01289, 2024.

Yu, X., Canadell, J. G., Henze, D. K., Patra, P. K., Saunois, M., Cen, X., Lan, X., Riddell-Young, B., Röckmann, T., and Jackson, R. B.: Incorporating methane isotopologues alters tropical and subtropical methane emission estimates, Nature Communications, 17, https://doi.org/10.1038/s41467-026-72668-2, 2026.

Zhang, Y., Cooper, O. R., Gaudel, A., Thompson, A. M., Nédélec, P., Ogino, S.-Y., and West, J. J.: Tropospheric ozone change from 1980 to 2010 dominated by equatorward redistribution of emissions, Nature Geoscience, 9, 875–879, https://doi.org/10.1038/ngeo2827, 2016.

Zhang, Z., Poulter, B., Feldman, A. F., Ying, Q., Ciais, P., Peng, S., and Li, X.: Recent intensification of wetland methane feedback, Nature Climate Change, 13, 430–433, https://doi.org/10.1038/s41558-023-01629-0, 2023.

Zhao, J., Ciais, P., Chevallier, F., Canadell, J. G., van der Velde, I. R., Chuvieco, E., Chen, Y., Zhang, Q., He, K., and Zheng, B.: Enhanced CH4 emissions from global wildfires likely due to undetected small fires, Nature Communications, 16, https://doi.org/10.1038/s41467-025-56218-w, 2025a.

Zhao, Y., Saunois, M., Bousquet, P., Lin, X., Berchet, A., Hegglin, M. I., Canadell, J. G., Jackson, R. B., Deushi, M., Jöckel, P., Kinnison, D., Kirner, O., Strode, S., Tilmes, S., Dlugokencky, E. J., and Zheng, B.: On the role of trend and variability in the hydroxyl radical (OH) in the global methane budget, Atmospheric Chemistry and Physics, 20, 13 011–13 022, https://doi.org/10.5194/acp-20-13011-2020, 2020.

Zhao, Y., Zheng, B., Saunois, M., Ciais, P., Hegglin, M. I., Lu, S., Li, Y., and Bousquet, P.: Air pollution modulates trends and variability of the global methane budget, Nature, 642, 369–375, https://doi.org/10.1038/s41586-025-09004-z, 2025b.

Zheng, B., Chevallier, F., Yin, Y., Ciais, P., Fortems-Cheiney, A., Deeter, M. N., Parker, R. J., Wang, Y., Worden, H. M., and Zhao, Y.: Global atmospheric carbon monoxide budget 2000–2017 inferred from multi-species atmospheric inversions, Earth System Science Data, 11, 1411–1436, https://doi.org/10.5194/essd-11-1411-2019, 2019.

Zhu, Q., Peng, C., Ciais, P., Jiang, H., Liu, J., Bousquet, P., Li, S., Chang, J., Fang, X., Zhou, X., Chen, H., Liu, S., Lin, G., Gong, P., Wang, M., Wang, H., Xiang, W., and Chen, J.: Interannual variation in methane emissions from tropical wetlands triggered by repeated El Niño Southern Oscillation, Global Change Biology, 23, 4706–4716, https://doi.org/10.1111/gcb.13726, 2017.

Zhu, Q., Neumann, N., Fiore, A. M., Pincus, R., Guan, J., Milly, G., Singer, C. E., Medeiros, B., and Giani, P.: Uncertain Natural Emissions Dampen the Increase in Tropospheric Hydroxyl Radical (OH) With Idealized Surface Warming, Journal of Advances in Modeling Earth Systems, 18, https://doi.org/10.1029/2025ms005248, 2026.